Effect of Residual Oil Saturation on Oil Recovery and Reservoir Performance for Mishrif Formation in Southern Iraqi Oil Field

AbdulKareem Abbas Khalil, Kerbala University, Kerbala City, Iraq; **Hussein Ali Baqer,** Almaaqal University, Basrah, Iraq; **Hiba Alaa Naseef,** University of Baghdad, Baghdad, Iraq; **Ahmed N. Al-Dujaili*,** Amirkabir University of Technology, Tehran, Iran

Abstract

The determination of the residual oil saturation (SOR) is an essential parameter for reserve assessment and recovery estimates. Moreover, reliable SOR data is crucial for potential incremental analysis under Enhanced Oil Recovery (EOR) methods. The objective of this study is to construct a reservoir model for the Buzurgan field in southeastern Iraq that aligns with actual field data measurements, predicts reservoir performance from 2007 to 2032, and determines the effect of the SOR on oil recovery using Petrel^{TM}. The matching percentage results were 100% after modifying the permeability and multiplying by 1.5, considering a weak aquifer that had not been considered previously. The predicted performance indicated a decrease in production rate and an increase in water cuts due to a significant decline in pressure. The proposed prediction strategy involves developing the capacity of surface facilities. The simulation model was executed to estimate the cumulative oil production and oil recovery for various SOR values (0.16, 0.23, 0.20, and 0.28), which results in a decline in recovery as SOR increases, due to changes in relative permeability. The secondary mechanism, implemented through injection, is used to enhance the recovery factor, increase productivity, and maintain pressure above the saturated pressure.

Introduction

The reservoir requires exploration and development to enhance recovery rates and reduce costs. Exploration will be conducted by geologists to gather data, while development may involve increasing the number of drilling wells or enhancing recovery through fracturing, acidizing, and injection (Satter and Iqbal 2015). The integration of reservoir studies encompasses defining and describing the reservoir structure, rock properties, fluid properties, and creating a reservoir simulation model (Al-Dujaili et al. 2024). Carbonate reservoirs pose greater challenges in estimating petrophysical properties and understanding fluid flow mechanisms and production performance compared to most sandstone reservoirs, due to their heterogeneous porosity and permeability distributions (Hurley et al. 1998). These reservoirs are highly complex, and proposing the correct reservoir model involves significant difficulties; thus, only limited success can be achieved with available and suitable reservoir simulation techniques. Field development planning is one of the most critical activities in reservoir engineering. The recovery strategy primarily depends on the geological characteristics of the reservoir and the operational schedule for the field (Al-Dujaili 2023). However, evaluating all possible combinations is not feasible due to the multitude of parameters influencing the decision-making process. Therefore, it is necessary to assess the most critical parameters related to the problem and develop an approach to achieve a satisfactory outcome (Cao et al. 2024).

A reservoir model represents the physical space of the reservoir through an array of discrete cells, defined by a grid that can be regular or irregular (Ugwu et al. 2023). Typically, this array of cells is three-dimensional, although one-dimensional and two-dimensional models are sometimes utilized. Each cell is associated with values

Improved Oil and Gas Recovery
DOI: 10.14800/IOGR.1366
Received February 3, 2025; revised June 21, 2025; accepted July 23, 2025.
*Corresponding author: ahmed.noori203@aut.ac.ir

for attributes such as porosity, permeability, and water saturation (Ugwu et al. 2023). The value of each attribute is assumed to be uniformly distributed throughout the volume of the reservoir represented by the cell. Geological models are constructed by geologists and geophysicists to provide a static description of the reservoir before production begins. Reservoir simulation models are developed by reservoir engineers and employ finite difference methods to simulate fluid flow within the reservoir throughout its production lifecycle (Aljawad et al. 2017). Effective attribute values for the simulation model are derived from the geological model through a process known as "upscaling." Alternatively, if a geological model is unavailable, attribute values for the simulation model can be determined by sampling geological maps (Hamdan 2011). The term "reservoir characterization" is sometimes used to describe reservoir modeling activities up until the point when a simulation model is prepared to simulate fluid flow. Commercial software is utilized in the construction, simulation, and analysis of reservoir models (Natvig et al. 2023).

The residual oil saturation (SOR) is the level of oil saturation above which the oil becomes movable. In petroleum reservoirs, only a small fraction of the original oil-in-place is economically recoverable through primary, secondary, and tertiary recovery methods. The oil that remains in the porous media after waterflooding is referred to as the remaining oil saturation (ROS), which is higher than the relative permeability residual oil saturation (Sorw or simply S_{or}). This residual oil saturation varies based on factors such as lithology, pore size distribution, permeability, wettability, fluid characteristics, recovery method, and production scheme. (Teklu et al. 2013) The determination of a reservoir's residual oil saturation is a critical parameter for reserve assessment and recovery predictions (Chen et al. 2023). Moreover, reliable SOR data is essential for evaluating potential incremental recovery through Enhanced Oil Recovery (EOR) techniques (Vishnumolakala et al. 2020). Core analysis offers direct measurement of reservoir properties. The laboratory-measured residual oil saturation from cores is contingent upon the method of core recovery and handling, including conventional coring, pressure coring, or sponge coring (Al-Dujaili et al. 2021a). Special core analysis (SCAL) encompasses all core analysis techniques beyond porosity and permeability measurements (Al-Dujaili et al. 2021b).

Cutoffs are limiting points at which the flow of fluid is halted. Each layer has specific cutoffs for petrophysical properties, including porosity, permeability, and water saturation (Zeyghami and Taghizadeh, 2023). Reservoirs with higher porosity and permeability can produce fluids (oil, gas, or water) with commercial productivity. In contrast, reservoirs with porosity and permeability values below the cutoff will not yield fluids of commercial value. The cutoff is crucial for estimating the volume of rocks that do not significantly contribute to the reservoir's evaluation (Worthington and Cosentino 2005) (**Figure 1**). The properties of the production zone should meet the following criteria: Porosity > cutoff, Permeability > cutoff, and Water Saturation < cutoff. Gross thickness is defined as the interval from the top to the bottom of the reservoir, encompassing all non-reservoir rocks such as shales, anhydrites, and salts. Net sand refers to the fraction of the gross sand that is porous, permeable, and contains hydrocarbons and water, subject to a defined or arbitrary porosity cutoff (Cobb and Marek 1998). Net pay is the component of the net sand that contains only hydrocarbons, subject to a water saturation cutoff. In addition to volumetric analysis, estimating net pay is useful for determining the total reservoir energy, which must account for both movable and non-movable hydrocarbons. The selection of net pay favors intervals with favorable relative permeability to injection fluids (Qassamipour et al. 2020).

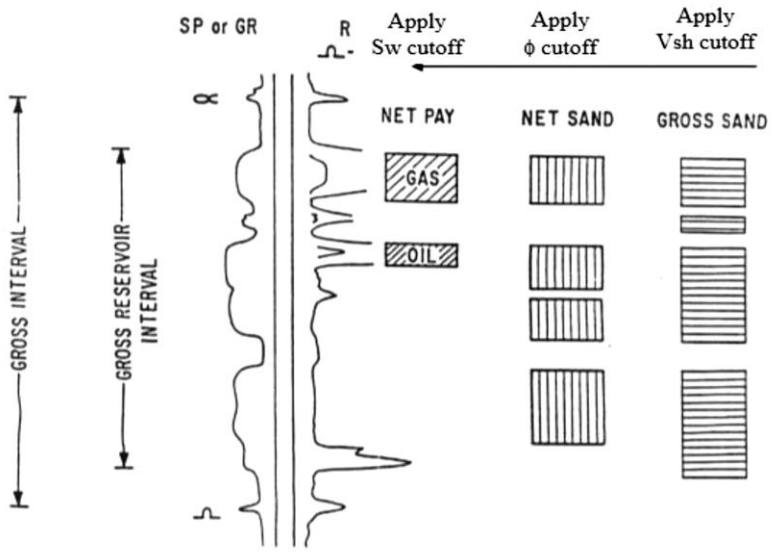

Figure 1—Reservoir interval pattern (Worthington and Cosentino 2005).

In water-wet rock, a layer of water coats the rock surface, acting as a lubricant for oil residing in the central parts of the pores. S_{wc} represents the connate or irreducible water saturation, which is the minimum water saturation at which water remains immobile due to capillary forces. The relative permeability of water at saturations below S_{wc} is zero. S_{orw} denotes the residual oil saturation or critical oil saturation, which is the minimum oil saturation at which the oil becomes immobile, meaning its relative permeability is zero, as depicted in **Figure 2** (Geffen et al. 1951; Eliebid et al. 2024).

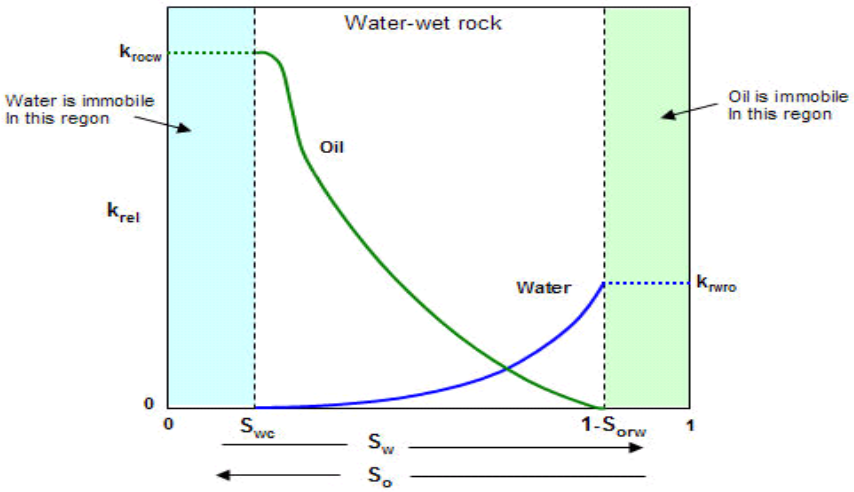

Figure 2—Oil-water relative permeability curves (Geffen et al. 1951).

Capillary pressures arise at the interfaces between two immiscible fluids within the pores (capillaries) of reservoir rock (Tsuji et al. 2016). Typically, one fluid phase is considered the wetting phase, while the other is the non-wetting phase. Consequently, drainage data can often be employed to forecast the saturation of non-wetting fluids at various points within a reservoir. In contrast, imbibition data can be valuable for evaluating the relative influences of capillary and viscous forces in dynamic systems (Muskat 1949). The Leverett 'J' function aims to correlate capillary pressure with pore structure, which is defined by porosity and permeability. The fundamental capillary model suggests that displacing a wetting phase with a non-wetting phase is predictable (Leverett and Lewis 1941).

$$J(sw) = 0.21645\, P_c/\sigma/ (\sqrt{k\emptyset}), \quad (1)$$

where J(sw) is the dimensionless J-function; P_c is the capillary pressure, in psi; σ represents the interfacial tension, in dynes/cm; k is the permeability, in md; and ∅ is the porosity, as a fraction.

Geological Setting

The Buzurgan Oil Field is situated in southeastern Iraq, close to the Iraqi-Iranian border, approximately 60 kilometers southeast of Amara City, the capital of Maysan Governorate. Structural contour maps of the Mishrif formation indicate that Buzurgan is an anticline fold with a length of 60 kilometers and a width of 8 kilometers (**Figure 3**) (Al-Mimar et al. 2015). Discovered in 1969, the field commenced production from the Mishrif reservoir in November 1976, utilizing a regular well pattern with large spacing (over 800 meters) (Seismic study for Buzergun and Fauqa oil field, 1980). The Buzurgan field comprises three primary formations: the Mishrif, Khasib, and Rumaila Formations. The Mishrif Formation, dating back to the Cretaceous period, is a key carbonate reservoir in southern Iraqi oil fields, recognized for its varied and complex features. Within this formation, six distinct facies have been identified, ranging from mid-decline to peripheral facies (Al-Dujaili et al. 2023a). Overlying the Mishrif Formation is the Khasib Formation, which acts as a cap rock for the Mishrif, and underlying it is the Rumaila Formation (Al Ibrahim et al. 2022). The Mishrif structure is segmented into three parts: the north dome, south dome, and saddle. The Mishrif formation consists of six units, MA, MB11, MB12, MB21, MC1, and MC2, owing to differences in composition, petrophysical properties, and fluid properties among them (Al-Mimar et al. 2018).

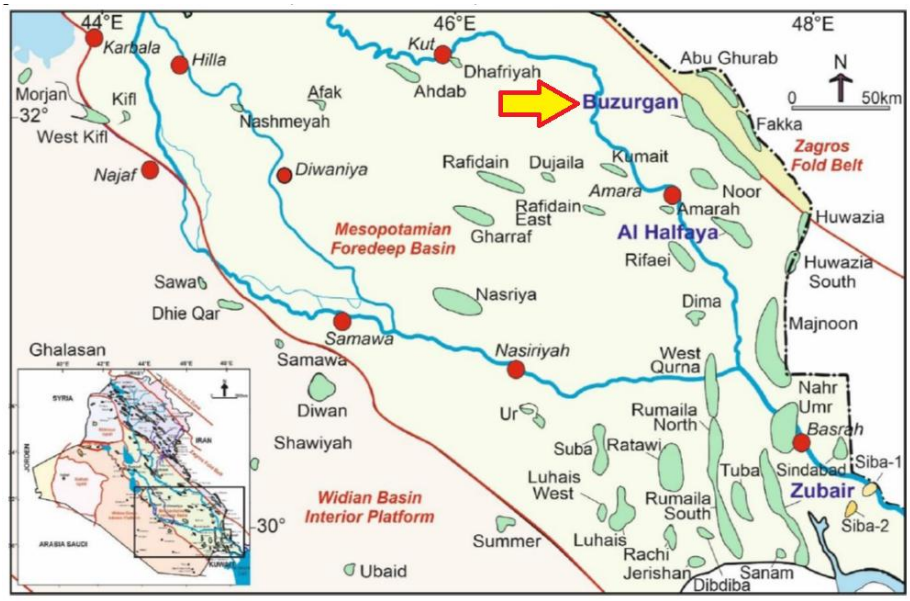

Figure 3—Location maps of the Buzurgan oilfield (Al Ibrahim et al. 2022).

Methodology

The data used included the final well report, which detailed the hole size, casing size, location, type of drilling mud, type of cementing, type of completion, and total depth for all wells. Additionally, the final geological report provided depth and thickness of formations for all wells. The CPI report, which stands for computer processing interpretation, encompassed log files for porosity and saturation data for wells BU-1, 6, 7, 12, 14, 15, and BU-16. The Core analysis report included porosity and permeability core data for wells BU-1, 2, 3, 4, 5, 6, 7, 10, 11, 12, 14, 15, and BU-18. The Special core analysis report detailed relative permeability and capillary pressure curves

for wells BU-3 and BU-4. PVT data, including pressure, formation volume factor, viscosity, density, and Gas Oil Ratio (GOR), was provided for wells BU-1, 3, 4, 6, 10, 12, 15, and BU-16. Lastly, daily production data from 1978 to 2007 was also included.

The general methodology for creating an adequate geological and reservoir model for the Mishrif Formation/Buzurgan Oilfield is organized as follows:

1. The Static Model is based on field data analysis to determine the Original Oil in Place (OOIP).
2. A dynamic model, developed to enhance a tool for predicting hydrocarbon reservoir performance under various operating strategies (Aziz, 1979), was constructed using dynamic data, such as PVT (Pressure-Volume-Temperature) and SCAL (Special Core Analysis) data, and subsequently simulated by the reservoir engineer.
3. Initial conditions, (including initial reservoir pressure, datum pressure, fluid contact, and aquifer properties, were used to solve the simulation model. SOR (Solution Gas-Oil Ratio) estimation was conducted using relative permeability curves for all cores. Following this, the simulation case must be executed for each SOR value to calculate cumulative production and recovery.

Initialization of Saturation and Pressure. Initialization involves assigning initial saturation and pressure values to each grid block within a reservoir, whether it contains hydrocarbons or not. The initial phase distribution is established based on the equilibrium between capillary pressure and gravitational force (Siripatrachai et al. 2017). The subsequent step may illustrate the workflow of the equilibrium method for an oil-water reservoir system, with the pressure datum depth situated in the oil zone. This workflow utilizes the Eclipse simulator (Alkhateeb 2019).

1. Identification the water pressure at reference point (OWC),

$$PW = PW, OWC @ Z = OWC , \quad (2)$$

2. At the OWC, PC=PD (the capillary enters pressure) PO=PW, WOC+PD
3. Estimation the hydrostatic head,

$$Po^i = PO, owc + \rho O\ g\ (Z^i - Zwoc), \quad (3)$$

$$Pw^i = Pw, owc + \rho w\ g\ (Z^i - Zwoc), \quad (4)$$

4. Estimation the P_c at all depths,

$$Pc^i = Po^i - Pw^i , \quad (5)$$

5. Using the P_c values and curve to estimate saturation at each depth,

$$Pci = f\ (S^i w), \quad (6)$$

where P_w is water pressure; P_w (owc) is reference water pressure at water oil contact depth (OWC); P_o is oil pressure; ρ_w is water density; ρ_o is oil density; and P_c is capillary pressure.

The workflow depicted in **Figure 4** shows the initialization of pressure and saturation.

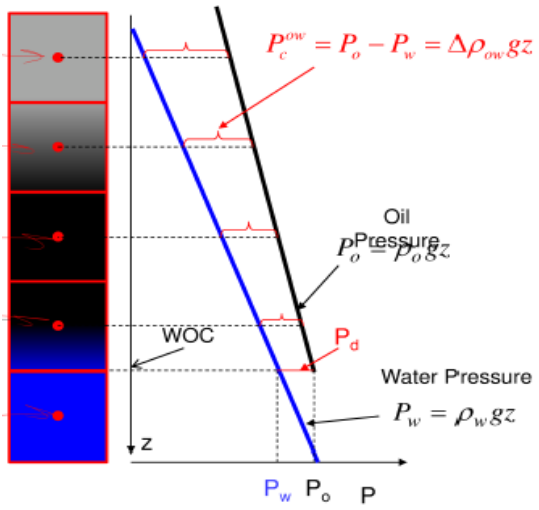

Figure 4—Initialization of pressure and saturation. (Alkhateeb 2019).

Capillary Pressure. Capillary pressure is crucial in reservoir engineering for controlling fluid distribution within reservoir rock (Ji et al. 2023). The small pores in reservoir rock act like capillary tubes and typically contain two immiscible fluid phases in contact (Deng et al. 2023; Al-Dujaili et al. 2023c). Numerous curves are involved in the calculation of capillary pressure for (BU-3 and BU-4), which arise from measuring capillary pressure using the restored state method (**Table 1**). Estimating the capillary pressure curve is essential for all reservoirs, as the core sample represents only a small portion of the reservoir. The Leverett J-function combines these curves. The Leverett J-function method can be estimated using the J-function method and plotted against water saturation to find the best-fit curve and subsequently calculate Pc for each (Jsw) (Tohidi et al. 2024).

Table 1—Core samples information for capillary pressure.

Sample No.	Well Name	Depth (m)	Porosity %	Permeability (m.d)
1	BU-3	12560	16.9	9.2
2	BU-3	12593	17.3	1.6
3	BU-3	12639	19.6	4.5
4	BU-3	12662	15.3	7.5
5	BU-3	12677	14.4	5.4
6	BU-4	12655	18.1	15.8
7	BU-4	12661	16.2	11.4
8	BU-4	12687	15.9	3.0
9	BU-4	12708	15.7	2.6
10	BU-4	12717	14.4	2.7

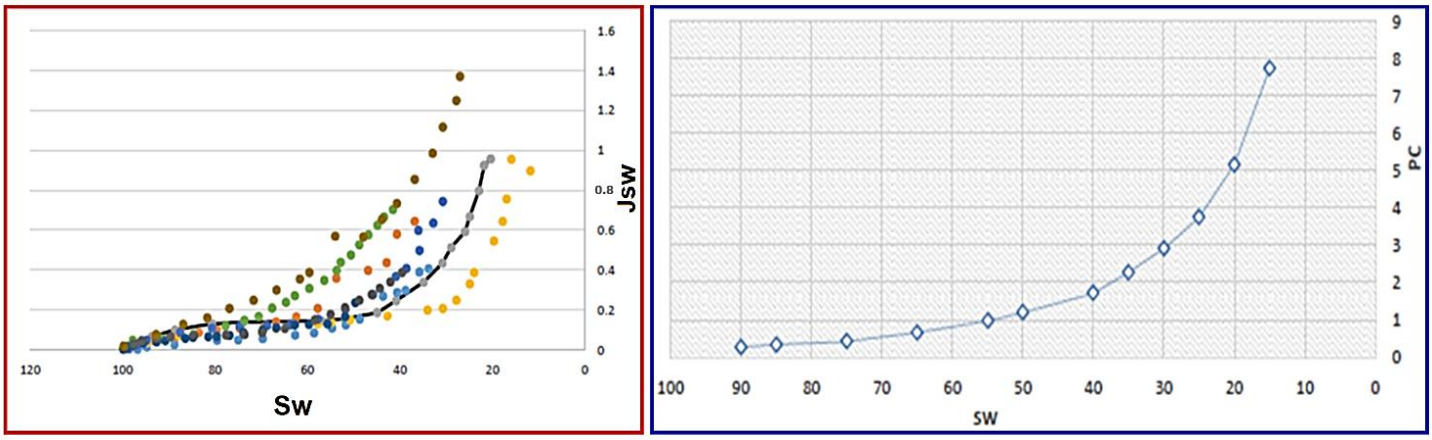

Figure 5—a)Relationship between SW vs J-function for all cores; b) Right- SW vs PC for all cores.

J_{sw} is calculated using **Eq. 1** at each water saturation (S_W), incorporating core sample properties such as porosity and permeability (Sugiharto et al. 2020). **Figure 5a** illustrates the scatter plot of J_{sw} against water saturation, along with the best-fit curve, which is drawn in black. Subsequently, Eq. 1 was applied using reservoir properties, including porosity and permeability, to determine p_c for each corresponding value of J_{sw} at a specific S_W (**Figure 5b**).

Fluid PVT Properties. Eight PVT samples were collected from wells (Bu1, Bu3, Bu4, Bu6, Bu10, Bu12, Bu15, and Bu16) at various depths, each with corresponding bottom-hole pressure values. To construct a PVT model, it is necessary to utilize a PVT program that employs standing correlations to track the average properties of the oil reservoir (Tariq and Abdulraheem 2021). **Table 2** presents the average properties of the PVT fluid.

Table 2—Average properties of PVT fluid.

Pressure (Kg/cm^2)	Bo (RB/STB)	GOR (m^3/ m^3)	Viscosity (CP)
56.9	1.13844	11.8633	3.06774
761.74	1.20105	37.4134	2.08431
1465.58	1.27351	64.2003	1.51324
2171.435	1.35981	94.3236	1.12725
2876.273	1.38005	105.403	1.0452
3581.125	1.38126	105.403	1.0884

Results and discussion

Static and Dynamic Geological Models. Petrel^{TM} comprises a suite of modules that derive their intrinsic capability to precisely characterize the reservoir by segmenting it into three-dimensional rock cells (Al-Dujaili et al. 2023c). The geo-modeling process has been developed in accordance with the Petrel workflow from Schlumberger Company, which integrates data to enhance 3D models of porosity, water saturation, and permeability estimates. This is achieved by incorporating well-bore petrophysical calculations and assigning properties through the appropriate application of deterministic, stochastic, and object modeling techniques (Mohammed et al. 2022) (**Figure 6**).

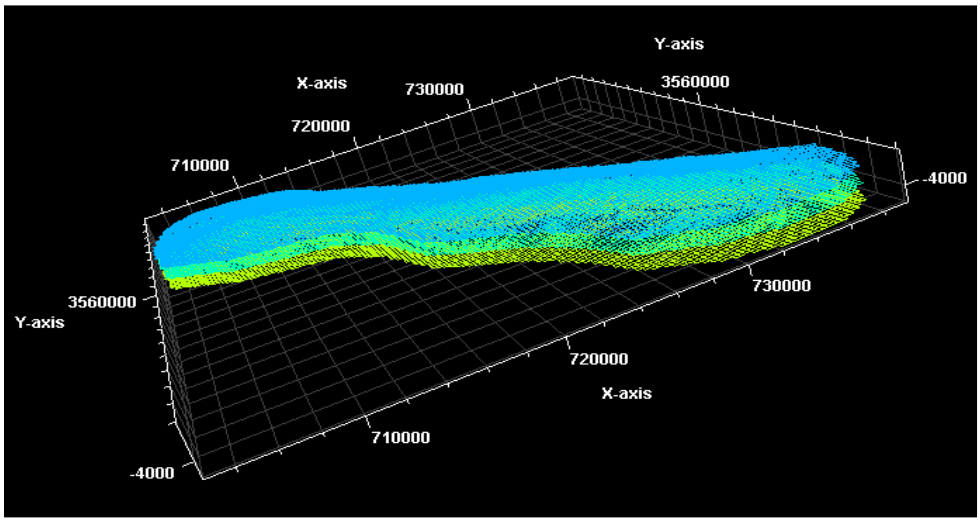

Figure 6—Skelton grid for the studied reservoir.

Stratigraphy. Stratigraphy seeks to ascertain the depth and thickness of reservoir units to facilitate correlation between wells (Mahmud et al. 2020). The stratigraphy of the Mishrif formation in the Buzurgan oil field has been subdivided into six units (MA, MB11, MB12, MB21, MC1, and MC2) based on previous studies and well reports. The boundaries of each unit were established through well-to-well correlation using Petrel software, which analyzed well logs and geological reports. **Figures 7** and **8** illustrate the well sections for wells BU-1, 3, 5, 6, 7, 10, 11, 14, 15, and BU-16.

The geological model was constructed using Petrel software, which performed the processes of horizon zoning and layering. **Figure 9** presents a 3D view of the Subsurface Units/Mishrif Formation, while **Table 3** details the average thickness and layer count for each reservoir unit.

Table 3—Division of vertical direction of 3D grid reservoir.

Zone	Unit	Thickness(m)	No. of Layers
Zone 1	MA-MB11	20	5
Zone 2	MB11-MB12	19-24	25
Zone 3	MB12-MB21	42-59	25
Zone 4	MB21-MC1	8-20	20
Zone 5	MC1-MC2	4-16	25

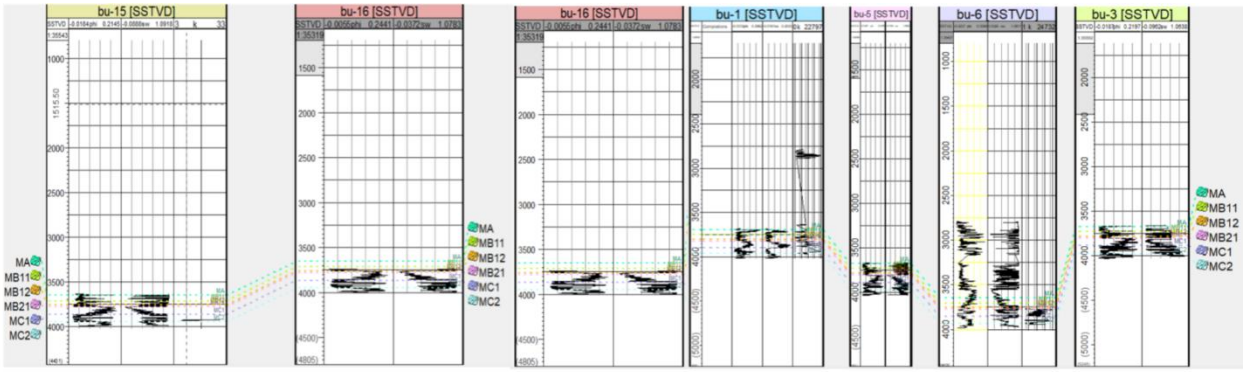

Figure 7—Well Section No.1 of Mishrif Zones and Layers.

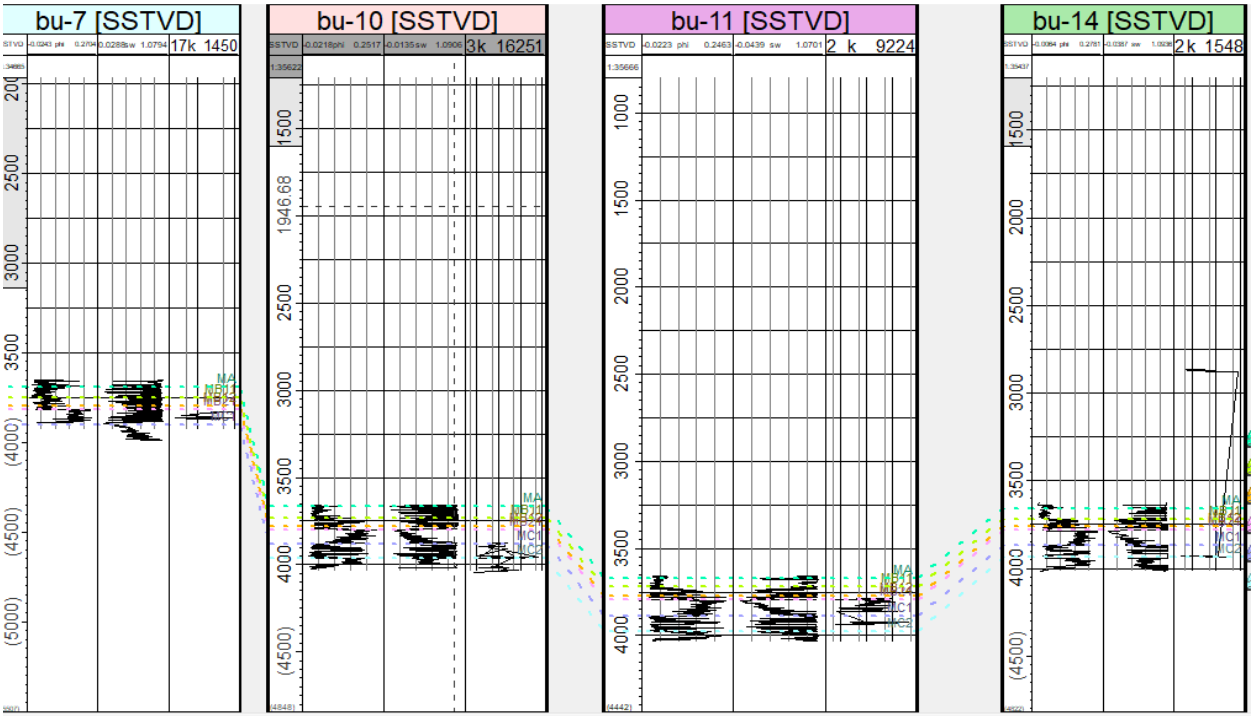

Figure 8—Well Section No.2 of Mishrif Zones and Layers.

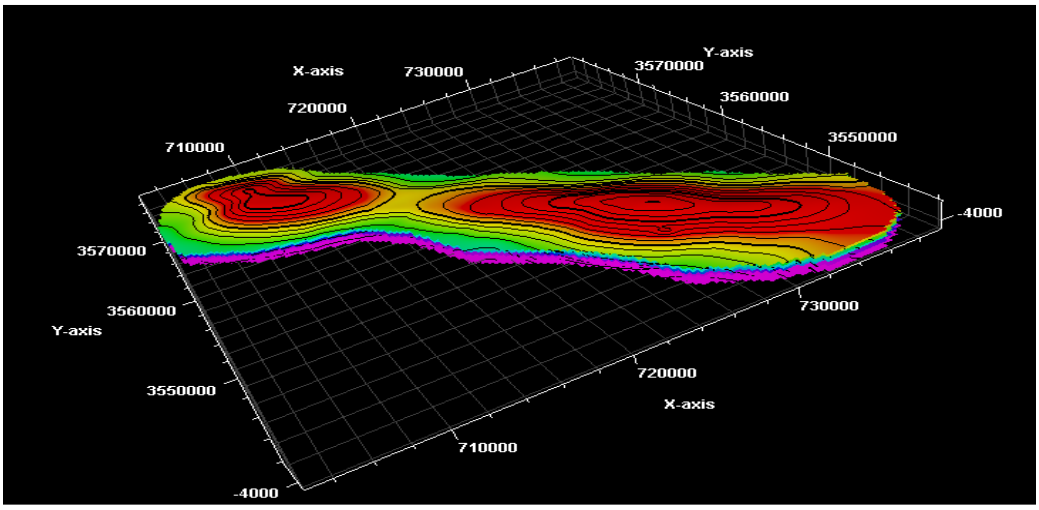

Figure 9—3D-View of Subsurface Units/ Mishrif Formation.

Property Modeling by Conventional Up-Scaling. The property modeling aims to distribute reservoir properties among wells to realistically describe the reservoir heterogeneity, matching the well data (Hamdi et al. 2014). The geological model must be upscaled for use in the reservoir simulator (Al-Janaee and Al-shahwan 2019). Upscaling, or homogenization, is the final stage of the geological model, involving the process of mathematically extrapolating fine-scale reservoir data to coarser scales to populate reservoir grid cells, which can be up to dozens of meters in size.

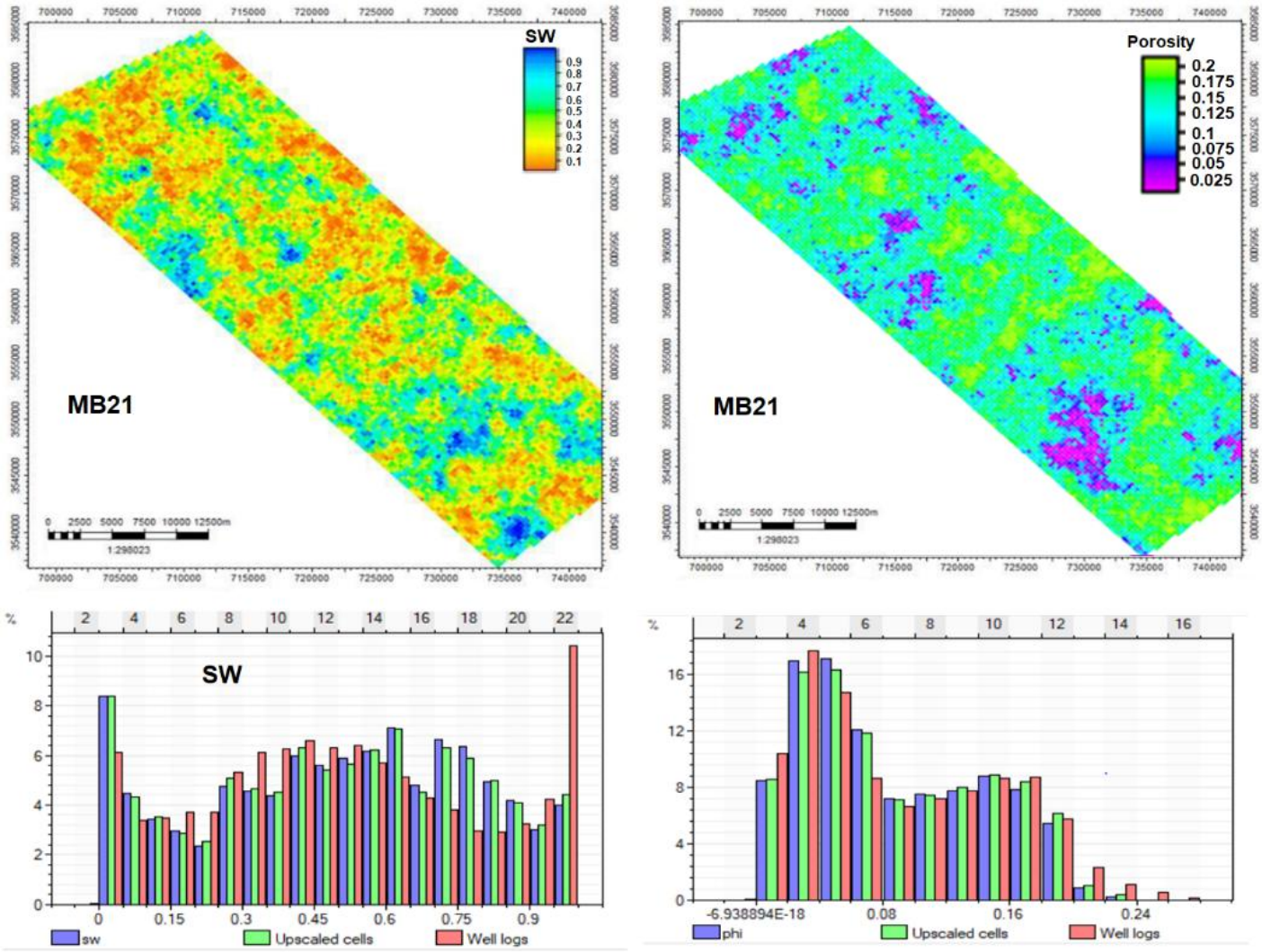

Figure 10—Top) Water saturation and porosity models of MB21 unit; Bottom) Water saturation and porosity histograms for all cells.

Static models for water saturation, porosity, and permeability were constructed using Petrel^{TM}, based on the CPI log data from wells BU-1, 6, 7, 12, 14, 15, and 16 in the Buzurgan oil field. The distribution of water saturation is used to estimate the original oil in place (OOIP), which is influenced by the capillary pressure curve (Alhusseini and Hamd-Allah 2022). The water saturation distribution is also affected by the oil-water contact, which is located 3860 feet below sea level (SL). The oil-water contact (OWC) value and two zones—the oil and water zones-were estimated in Petrel^{TM}. **Figure 10** illustrates the water saturation and porosity distribution maps for MB21, as well as histograms. The results indicate that porosity distribution values range from 0.012 to 0.1842 (**Table 4**), with water saturation values between 0.9 and 1.0 covering 45% of the cells, while the remaining 55% range from zero to 0.9 (Figure 10).

Table 4—Summary of statistical results of porosity distribution

Unit	Type	Min.	Max.	Delta	Mean	Std.
Zone 1	Property Upscale	0.0325 0.0325	0.1842 0.1842	0.1516 0.1516	0.1350 0.1350	0.319 0.316
Zone 2	Property Upscale	0.0121 0.0120	0.1523 0.1523	0.1401 0.1401	0.0559 0.0547	0.0322 0.0330
Zone 3	Property Upscale	0.0410 0.0410	0.1659 0.1659	0.1249 0.1249	0.0989 0.1043	0.0360 0.0370
Zone 4	Property Upscale	0.0310 0.0306	0.1432 0.1459	0.1122 0.1109	0.0867 0.0913	0.0370 0.0380
Zone 5	Property Upscale	0.0223 0.0226	0.1460 0.1406	0.118 0.118	0.127 0.109	0.0298 0.0288

The classic method was used as the basis for estimating permeability values, employing a cross plot between core porosity and permeability, based on conventional core analysis data. Porosity logs were used to set a permeability cut-off at 0.1 (Farouk et al. 2021). The unit MB21 is particularly crucial as it represents the reservoir units and has a significant impact on the dynamic model well-log interpretation. MB21 is characterized as sandstone, while the MC1 and MC2 units are predominantly shale sand and exhibit better porosity and permeability (**Figure 11**). Due to the discrepancy between core and log porosity, a mathematical correlation can be established to correct porosity values. Consequently, corrected porosity values, in conjunction with core permeability at a permeability cut-off of 0.1, can be depicted (**Figure 12** and **Table 5**).

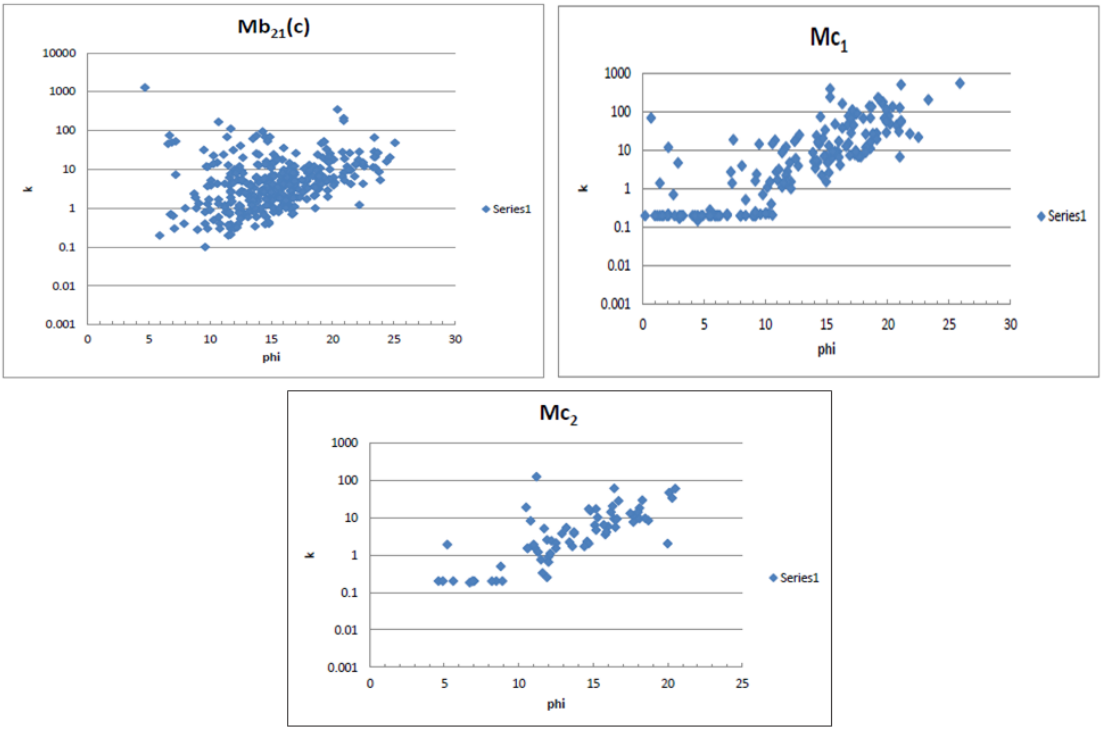

Figure 11—Scatter plot of porosity versus permeability for cores from the Mb21, Mc1, and Mc2 units.

Table 5—Properties cut-off value for each unit.

Unit	Permeability	Porosity
mB21	0.1	8.2
mC1	0.1	6
mC2	0.1	7.5

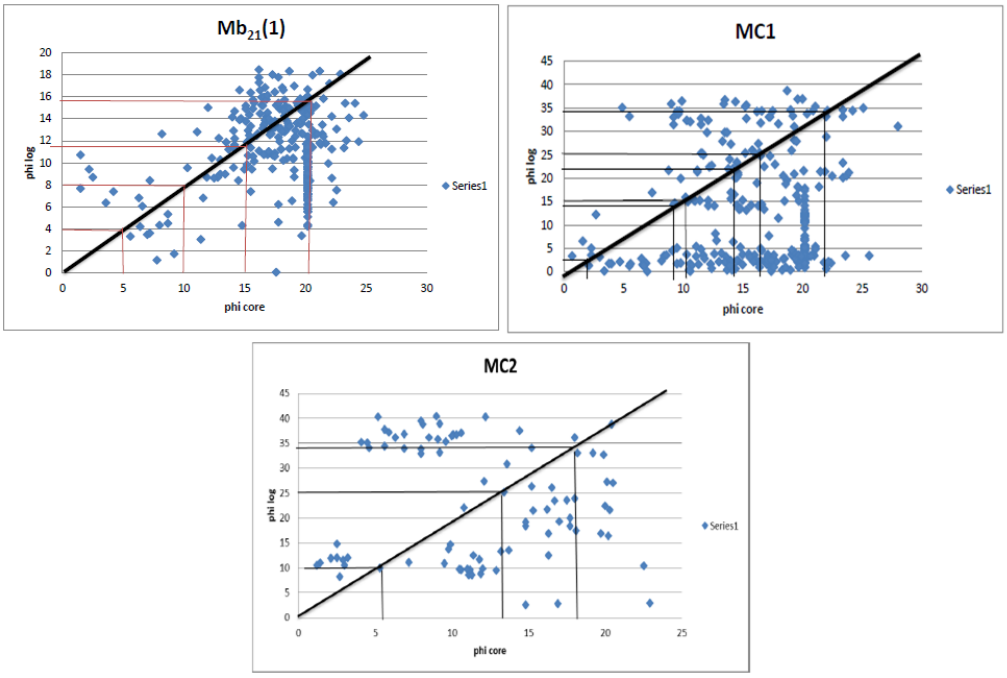

Figure 12—Scatter plot of porosity log versus porosity core for Mb21, Mc1, and Mc2 units.

Reservoir Interval Calculation. The reservoir interval encompasses all layers, both hydrocarbon-bearing and non-hydrocarbon-bearing, such as shale, anhydrites, salts, etc. (Liu et al. 2023). Net pay is crucial for assessing the total reservoir energy, which includes both mobile and immobile hydrocarbons. It can be estimated by considering the net-to-gross ratio, based on the threshold values for porosity and water saturation, while disregarding values that fall below these thresholds (Ebraheem et al. 2022). The reservoir interval can be delineated by the upper and lower boundaries of each layer, as identified by IP TM. **Table 6** presents the results of the reservoir interval analysis for each well.

Table 6—Reservoir interval calculation.

BU-1	N/G	Net	Gross	Bottom	Top	BU-3	N/G	Net	Gross	Bottom	Top
	1	77	77	3954.3	3877.3		0.988	83	84	3910.5	3826.5
	0.657	40.2	61.2	4015.5	3954.4		0.478	44	92.1	4002.6	3910.5
	0.965	42.5	45.5	4061	4015.5		0.945	32.5	34.4	4037	4002.6
BU-5	N/G	Net	Gross	Bottom	Top	BU-6	N/G	Net	Gross	Bottom	Top
	0.973	84.61	87	3912	3825						
	0.39	30.39	78	3990	3912		0.602	72	116.9	3878.5	3795.5
	0.7	26.61	38	4028	3990		0.602	72	116.9	4960	3878.5
BU-7	N/G	Net	Gross	Bottom	Top	BU-10	N/G	Net	Gross	Bottom	Top
	0.963	68	70.95	3926.5	3840.5		0.963	80	81.5	3903	3821.5
	0	0	0	4017.8	3926.5		0.509	43.55	85.5	3988.5	3903
	0	0	0	4065	4017.8		0.965	28	29	4017.5	3988.5
BU-11	N/G	Net	Gross	Bottom	Top	BU-12	N/G	Net	Gross	Bottom	Top
	0.978	89.51	91.5	3916.5	3825		0.976	73.2	75	3916	
	0.311	28	90	4006.5	3916.5		0.439	31	70.5	3986.5	3916
	0.97	32.49	33.5	4040	4006.5		0.969	32	33	4019.5	3986.5
BU-13	N/G	Net	Gross	Bottom	Top	BU-14	N/G	Net	Gross	Bottom	Top
	0.677	58.21	86	3887.5	3801.5		0.988	85.2	86.5	3893.5	3807
	0.525	42.79	81.5	3969	3887.5		0.89	60.1	67.5	3961	3893.5
	0.568	22.71	40	4009	3969		0.967	47.4	49	4010	3961
BU-15	N/G	Net	Gross	Bottom	Top	BU-16	N/G	Net	Gross	Bottom	Top
	0.972	83.64	86	3889	3803		0.951	79.43	83.5	3889.5	3806
	0.651	53.44	82	3971	3889		0.627	53.57	85.5	3975	3889.5
	0.989	35.52	36	4007	3971		1	34.5	34.5	4009	3975

Based on the porosity distribution maps for each unit, Unit MA exhibits low porosity due to the lithological heterogeneity between shale and sand. The MB21 unit, however, demonstrates excellent porosity values, while the MC unit has good porosity values. The net pay and net-to-gross models were constructed using Petrel™ (**Figure 13**).

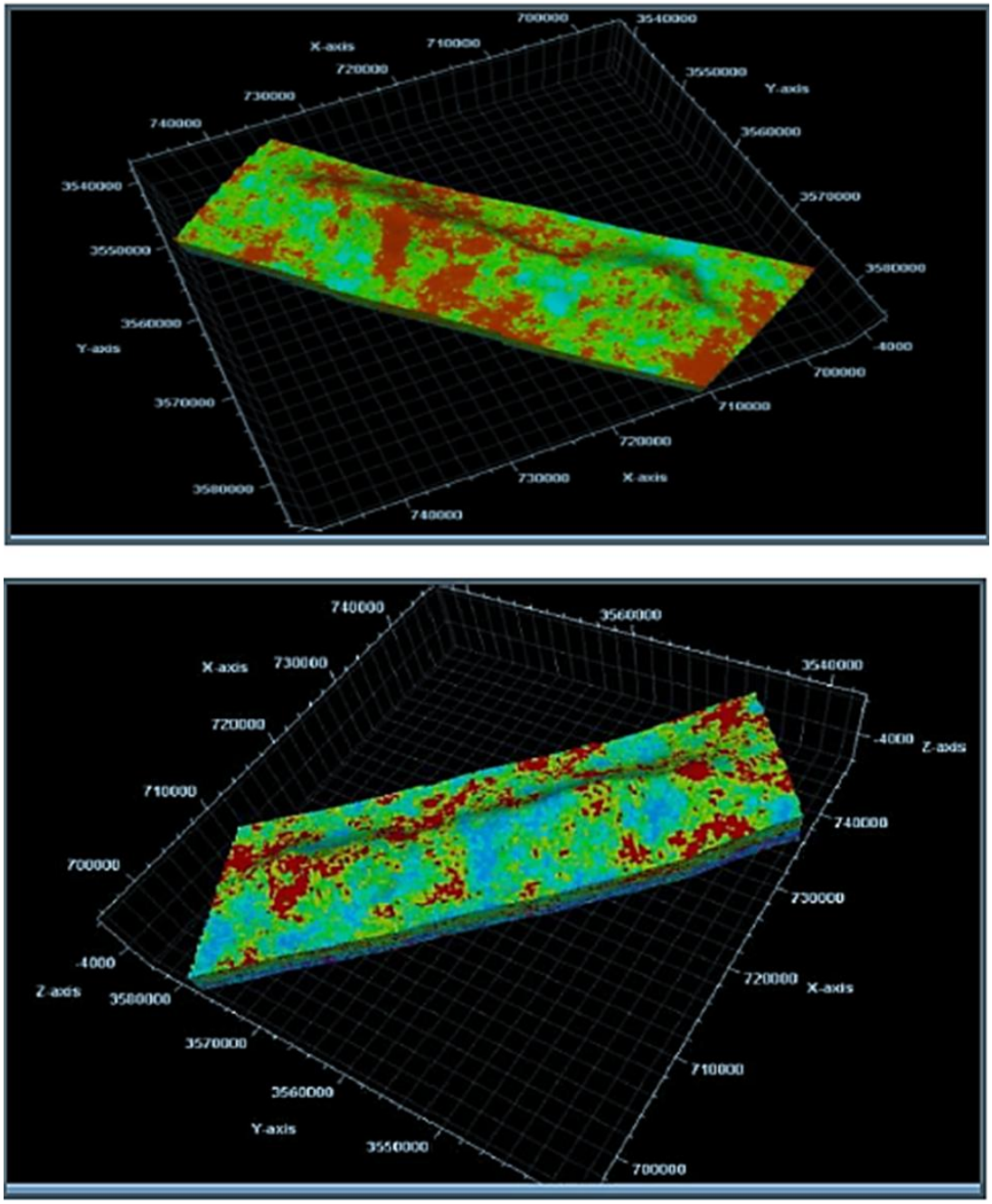

Figure 13—Top) Net to gross Map distribution; Bottom) Net pay map distribution for MB21 unit.

Dynamic Model. The dynamic model constitutes the second phase of this study, representing time-dependent elements. Petrel TM was utilized to construct this model, incorporating the oil-water relative permeability curve, the P_c curve, PVT data, and production data.

Relative Permeability. In this study, numerous relative permeability curves are presented for wells Bu-3 and Bu-4. Each well has multiple samples, with each sample possessing distinct porosity and permeability values. The average relative permeability for the water–oil system can be estimated (**Figure 14**).

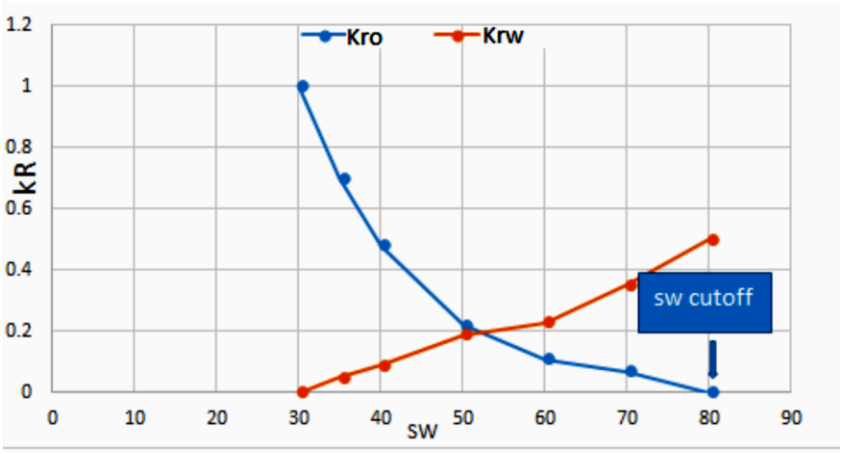

Figure 14—Average oil -water relative permeability curve.

Importing the PVT data into Petrel™ leads to the establishment and development of PVT and dynamic simulation models. **Figure 15** illustrates the correlations of (B_o, GOR, density, and viscosity) with pressure.

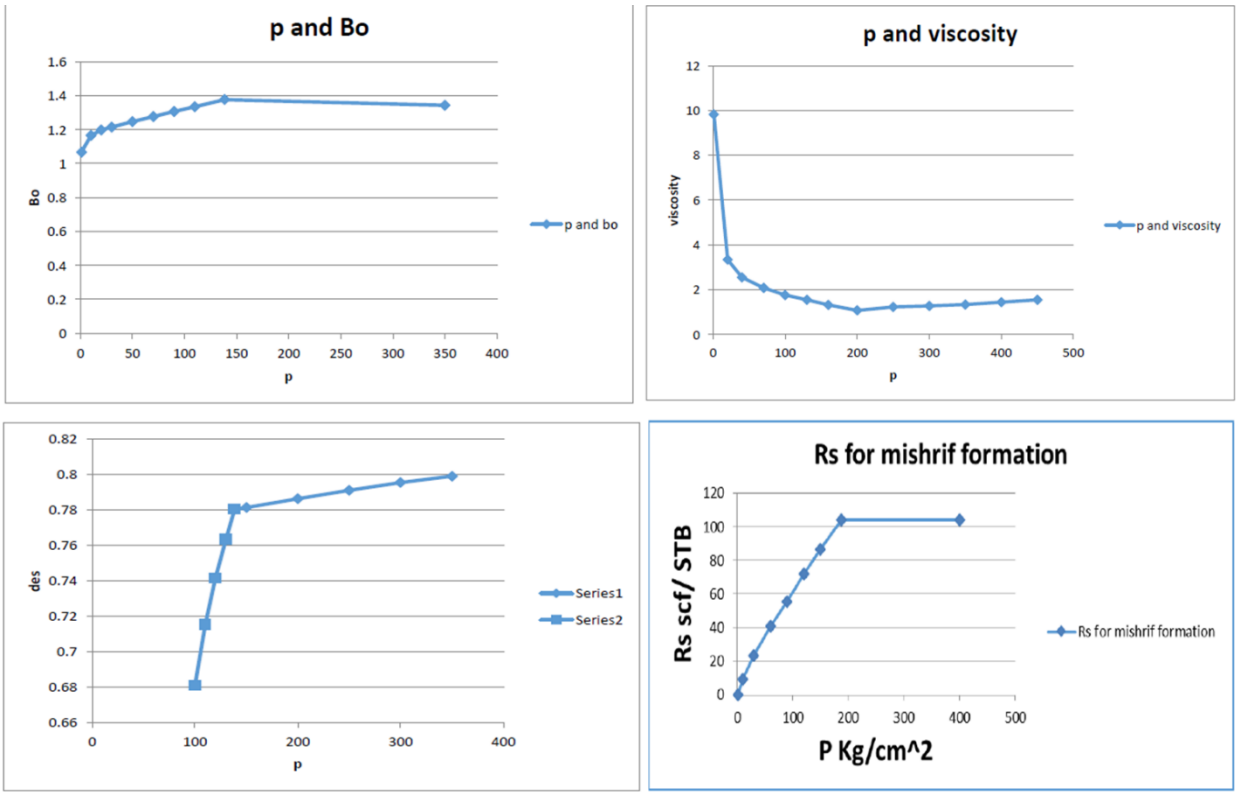

Figure 15—Averaging model for the formation volume factor, viscosity, density, and Rs.

Residual Oil Saturation Calculation. The residual oil saturation for wells BU-3 and BU-4 can be estimated through special core analysis tests. By utilizing the relative permeability curve from numerous samples, an average curve can be derived to estimate the relative permeabilities to oil (Kro) and water (Krw) at various water saturation levels (**Figure 16**). Given that the Sor (residual oil saturation) is 0.2, these results can then be applied to a simulation to project the accumulative production.

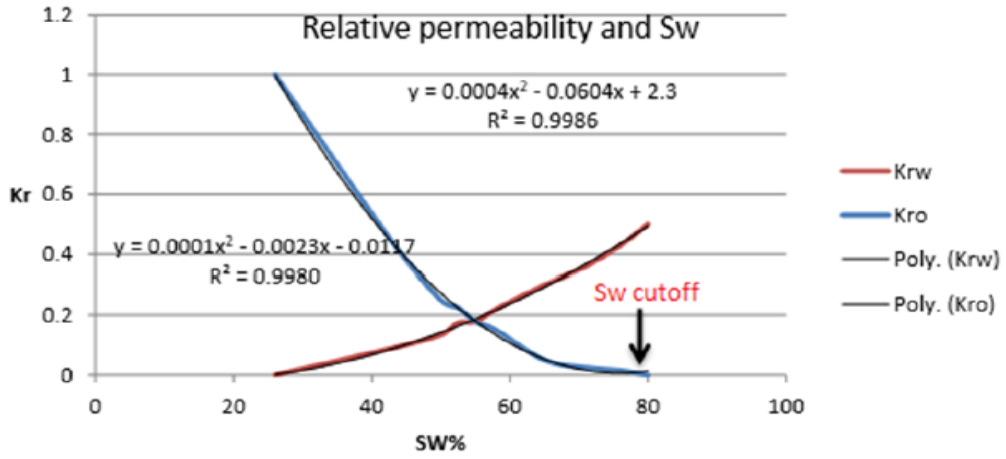

Figure 16—Relative permeability curve for estimating SOR.

The relationship between the recovery factor and the SOR can be summarized by altering the SOR values and adjusting the average curve at the S_W cutoff to 0.84. Subsequently, k_{ro} and k_{rw} are estimated at various water saturation levels. These estimates are then utilized to conduct another simulation run to calculate the accumulative production. **Table 7** presents the assumed SOR values, which are based on **Eq. 7**,

$$SOR = 1 - SW\ cutoff, \quad (7)$$

Table 7—Residual oil saturation value.

SW Cutoff	SOR
0.8	0.2
0.77	0.23
0.72	0.28

Simulation Model. Reservoir simulation is one of the most effective techniques currently available to reservoir engineers. The model requires that the field under study be described by a grid system, usually referred to (s cells or grid blocks. Each cell must be assigned to represent the reservoir properties. The simulation allows for the description of a fully heterogeneous reservoir, including varied well performance and studying different recovery mechanisms.

History Matching. The observed oil production rates (monthly measurements) were honored, along with the reservoir pressure measurements from static gradient surveys (a single value for each well's entire production history). However, the production history data (spanning a long period from 1976 to 2007) is available for wells BU-1, BU-3, BU-4, BU-5, BU-6, BU-7, BU-9, BU-10, BU-11, BU-12, BU-13, BU-14, BU-15, BU-16, BU-17, BU-18, BU-19, and BU-20 (refer to **Table 8**). The history matching, which encompasses both pressure and production history, was achieved by running the numerical model, iteratively adjusting the permeability distribution (multiplying permeability by a specific factor for all the reservoirs under study) until a satisfactory match was found between the measured and calculated production histories, while the porosity distribution was

derived from the geological model. **Figure 17** illustrates the matching of cumulative field oil production and field pressure, as calculated by Petrel^{TM}, along with the field recovery factor and pressure. **Figures 18** to **21** depict the historical matching of oil production rates for wells within the reservoir under study. The Buzurgan oil field commenced production in 1976 and continued until 1980, when production ceased in the field due to the Iraqi-Iran war. Production resumed in 1998 and has continued to the present day.

Table 8—Date of well history production data.

Well No.	History of Oil Production		Period (Months)	Oil rate (bbl/day)
	From	To		
BU-1	1/11/1976	1/1/1980	49	2750
	1/1/2000	26/9/2004	57	2590
BU-4	1/2/1976	1/2/1980	48	8000
	1/7/2004	31/7/2004	1	2350
BU-5	1/5/1976	1/1/1980	44	9050
	3/2/1999	5/4/2003	50	6400.3
BU-6	1/1/2002	1/7/2002	7	4409
BU-7	1/2/1977	1/1/1981	47	5120.6
BU-9	1/1/1977	23/6/1979	30	2500
	1/1/2000	15/1/2003	36	4600
BU-10	3/1/1978	11/1/1981	38	3800
	1/8/1998	14/7/2002	61	3450
BU-11	1/8/1980	2/11/1980	3	4450
	1/8/1998	14/7/2002	23	4000
BU-12	1/2/1999	12/11/2002	43	3400
BU-13	1/3/2000	1/1/2001	10	4900
	1/1/2002	1/9/2002	9	5250
BU-14	1/6/1980	1/11/1980	5	2200
	1/4/1999	1/6/2002	38	4050
BU-15	1/1/2003	1/1/2007	48	2350
BU-16	1/1/2000	1/7/2007	31	4450
BU-17	1/10/1980	31/10/1980	1	2780
	1/7/1998	1/7/2002	48	3080
BU-18	1/1/2003	1/1/2007	48	3300
BU-19	1/1/2001	1/10/2002	22	2600
BU-20	1/1/2000	1/1/2001	12	2350
	1/1/2002	1/6/2002	60	2550

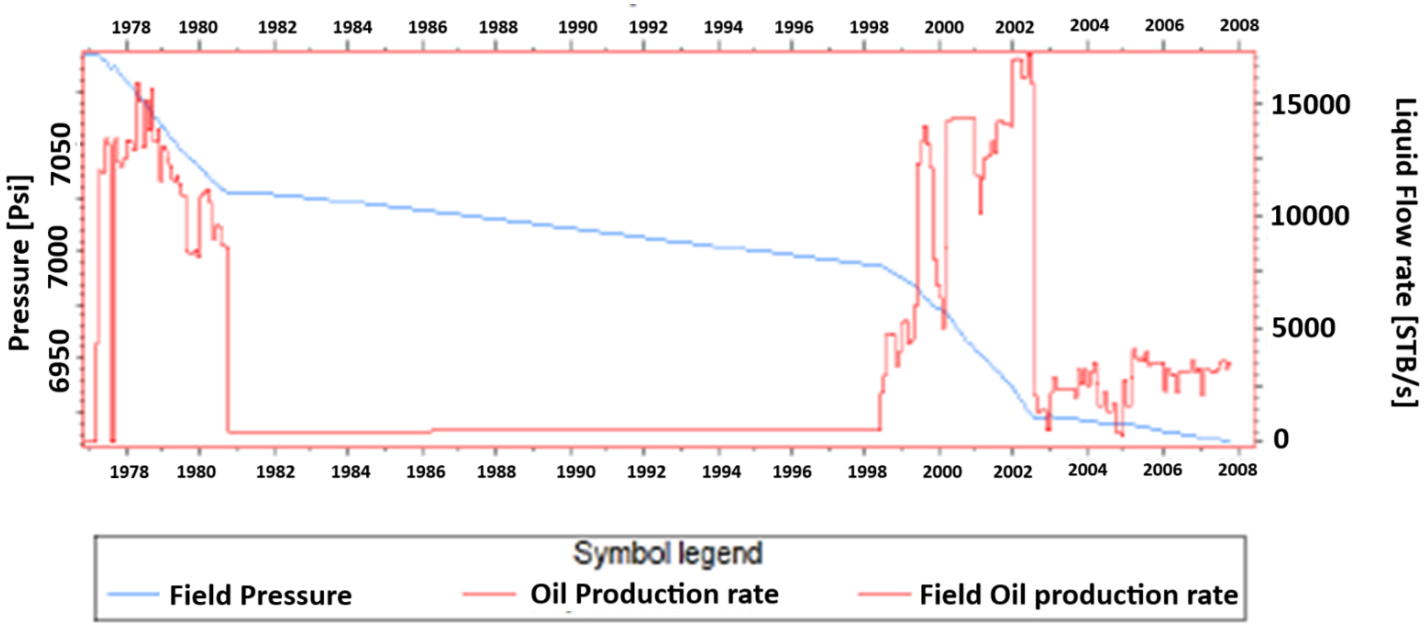

Figure 17—Field oil production rate (calculated vs. observed) with corresponding field pressure.

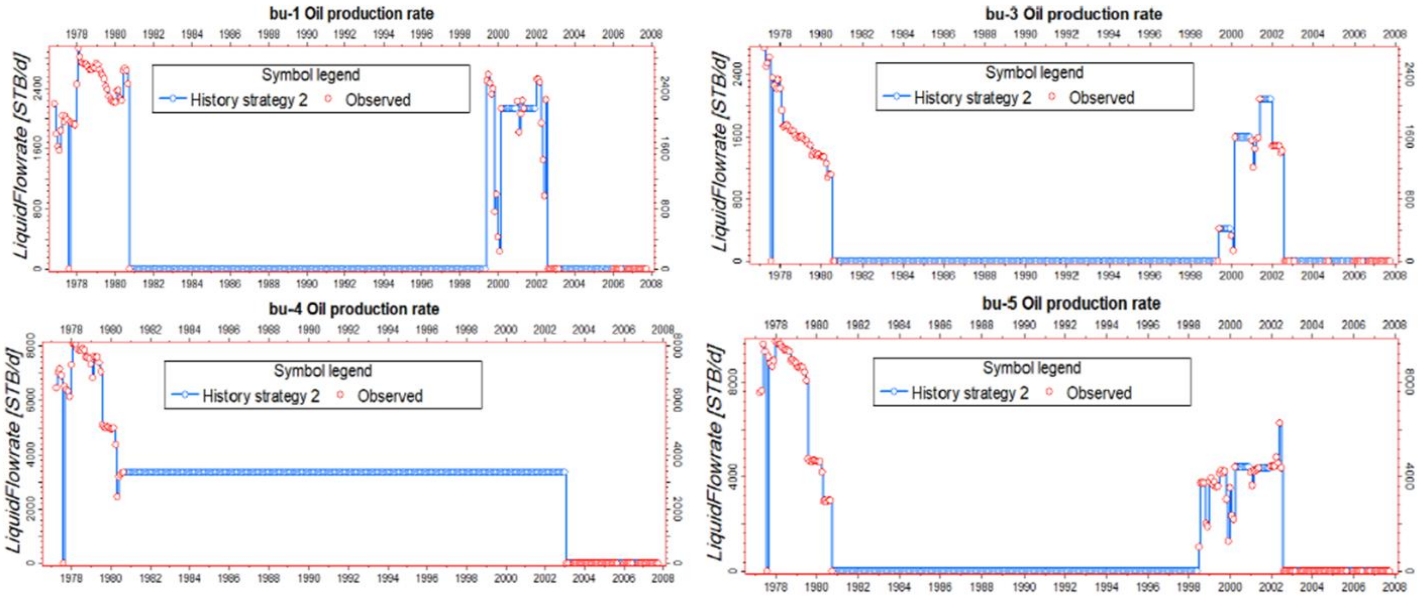

Figure 18—Oil production rate (calculated and observed) for Wells BU-1, 3, 4, and 5.

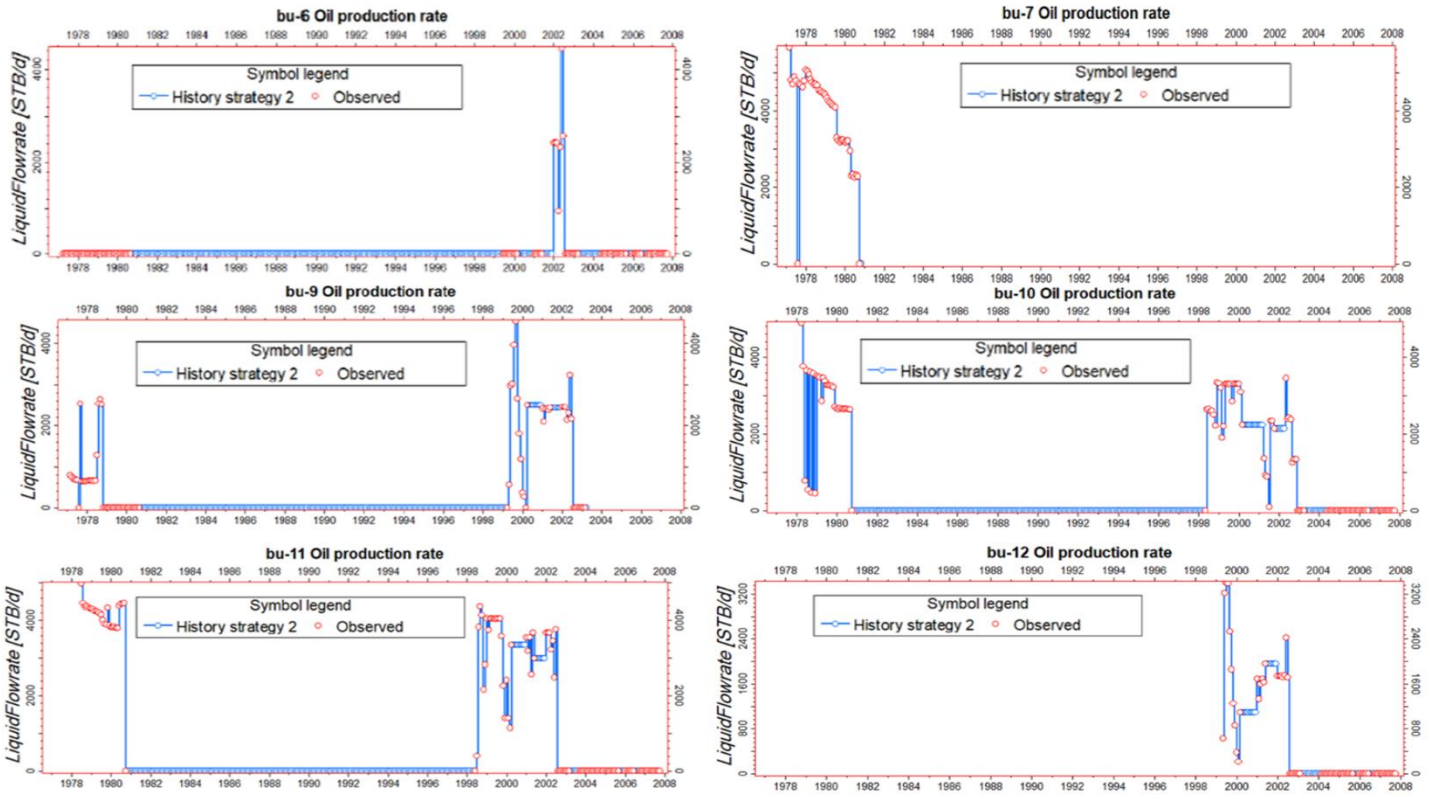

Figure 19—Oil production rate (calculated and observed) for the wells BU-6, 7, 9, 10, 11, and 12.

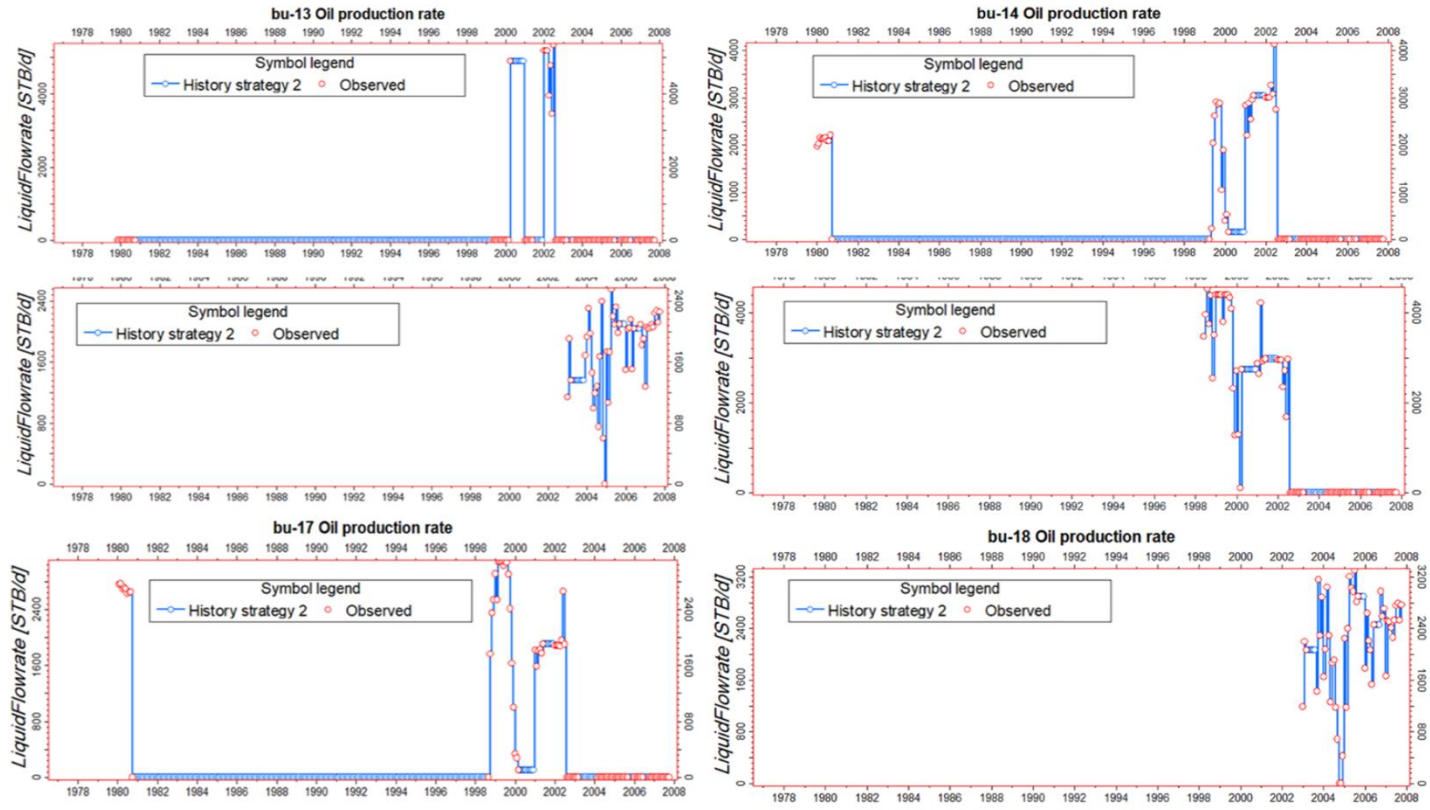

Figure 20—Oil production rate (calculated and observed) for the wells BU-13, 14, 15, 16, 17, and 18.

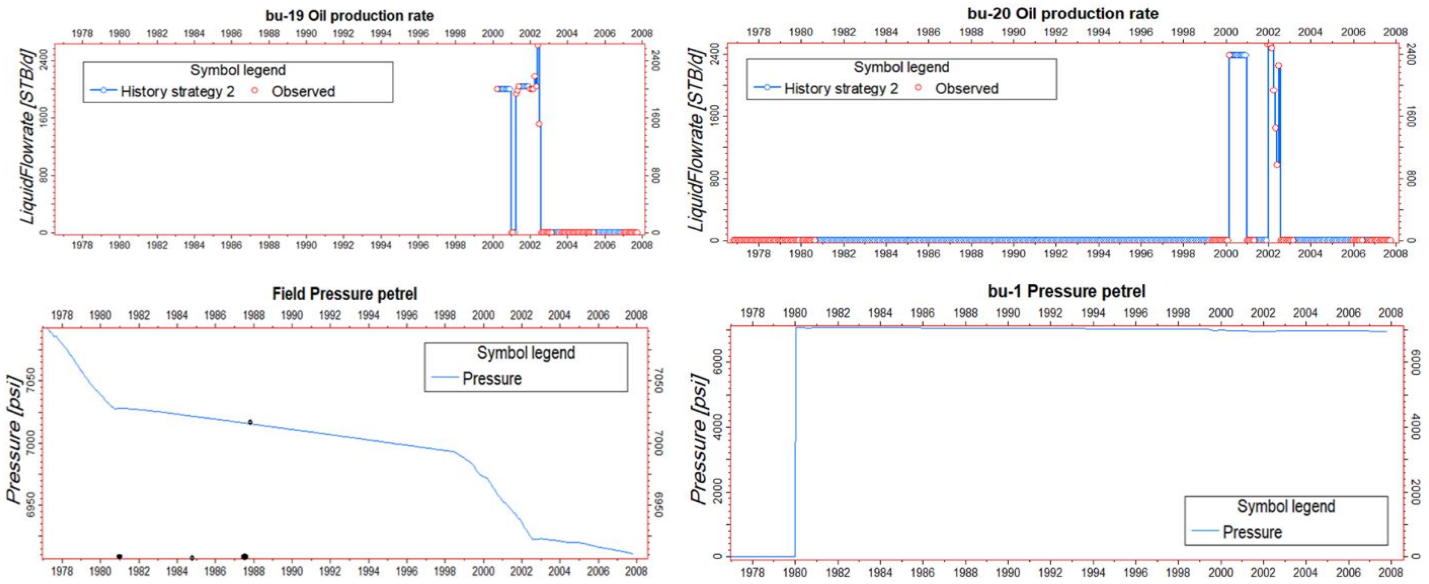

Figure 21—Oil production rate (calculated and observed) for the wells BU-19 and BU-20, calculated field pressure, and field pressure for the well BU-1.

Geological Structure. The geological structure of the Buzurgan oil field extends from the northwest to the southeast and comprises two domes. The southern dome is larger and higher than the northern dome. The primary producing reservoir within the Mishrif formation is the MB21 unit, which is the thickest and accounts for over 90% of production. It is more significant than the other units due to its favorable porosity (exceeding 6%) and low water saturation (below 60%), indicating economically viable oil reserves. Wells in this field produce naturally. Prior to 2003, 18 wells were drilled. After 2003, 44 directional wells were drilled primarily in the southern dome of the Mishrif structure to enhance productivity. No wells have been drilled in the area between the two domes, as it is a water saddle. Moreover, the southern dome's proximity to the surface suggests a greater potential for recovery.

The three units (MB21, MC1, and MC2) are more considerable in petrophysical properties. As compared between the three units in these properties for porosity cut-off (**Table 9**). These values show that Unit MC1 has more recoverable volumes. But these values are not absolute as compared to thickness, unit MB21 still gives more recoverable volumes.

Table 9—Porosity cut-off for Mishrif units.

Unit	MB21	MC1	MC2
Porosity cut off	8.2	6	7.5

Volume Calculations. Volume calculation involves estimating pore volume and determining the stock tank's original oil in place (STOOIP). The pore volume for each grid cell is calculated by multiplying the cell's volume (bulk volume) by its porosity. The (TOOIP is determined by multiplying the pore volume by the oil saturation and then dividing by the oil formation volume factor (Bo) for each grid cell. The total STOOIP is the sum of the STOOIP values across all the reservoir grid cells. The following equation illustrates these calculations.

$$STOOIP = \frac{V_{p*(1-S_W)}}{B_o}, \quad (8)$$

$$V_p = \emptyset * V_B, \quad (9)$$

where V_p is pore volume; V_B is bulk volume; Ø is porosity; S_w is water saturation; and B_o is formation volume factor.

The static and dynamic models estimate the initial oil in place. There were differences between the two values according to the method used in the cell porosity and saturation estimation, in addition to the Bo. Calculation with a static model depends on the cell value of the petrophysical model that was estimated from Well logs and distributed overall reservoir with Geo-statistics methods. The result value of STOOIP is (3.2 billion cubic meters) according to B_o value used.

For the dynamic model, the porosity differs from that of static because of the effect of rock compaction considering the rock compressibility effect represented by the pore volume at the reservoir pressure condition using the following equation:

$$\text{Vpore (p)} = \text{Vpore (Pref)} [1 + \text{C (P} - \text{Pref)}], \quad (10)$$

where V_{pore} (p) is the pore volume at cell pressure; V_{pore} (Pref) is the pore volume at reference pressure; C is the rock compressibility; P is cell pressure; and P_{ref} is reference pressure.

The method for distributing water saturation in the dynamic model differs from that in the static model. In the dynamic model, water saturation distribution relies on the capillary pressure curve. The oil formation volume factor (B_o) in the dynamic model is defined in relation to cell pressure and in accordance with the oil PVT table. The dynamic model's estimate of STOOIP is 2.1 billion cubic meters, which varies from the static model's estimate.

History Matching. AAfter constructing the reservoir model, the reservoir simulation model was executed to match the production and pressure history and to validate the constructed model. There are numerous simulation models that can be used to reach the match point. Each simulation model varies by altering the variables, including the reservoir characteristics (**Figure 22**). The blue solid line represents the calculated oil production rate by the simulation model operating in oil rate mode, alongside the observed production rate and without any alterations to the variables. The estimated rate did not align with the measured historical production data (depicted by the dotted red line) because of the declining bottom hole pressure (BHP).

The significant drop in bottom hole pressure (BHP) depicted in Figure 22 results in alterations to the well-control mode. The BHP control mode reduces the production rate to maintain BHP above the saturation pressure. There are several reasons for the high pressure decline, including the neglect of the aquifer effect (assuming the reservoir lacks aquifer support), its weakness, the absence of data, or uncertainties regarding reservoir permeability. Generally, history matching is an inverse problem that entails adjusting model parameters until the simulation output from the reservoir model aligns with observed data.

There are discrepancies between the observed and calculated values due to the significant decrease in bottom hole pressure (BHP) (refer to Figure 22). The additional aquifer increases the reservoir pressure at the measurement point, yet it fails to achieve a satisfactory match. On the other hand, reservoir properties are the primary factor influencing the production rate, with reservoir pressure being indicative of permeability. This is because increased permeability raises the flowing bottom hole pressure (FBHP), allowing the well to continue producing under oil rate control, while the decline in reservoir pressure diminishes. Consequently, the horizontal permeability has been adjusted using a multiplier of 1.5. This adjustment falls within the range of uncertainty.

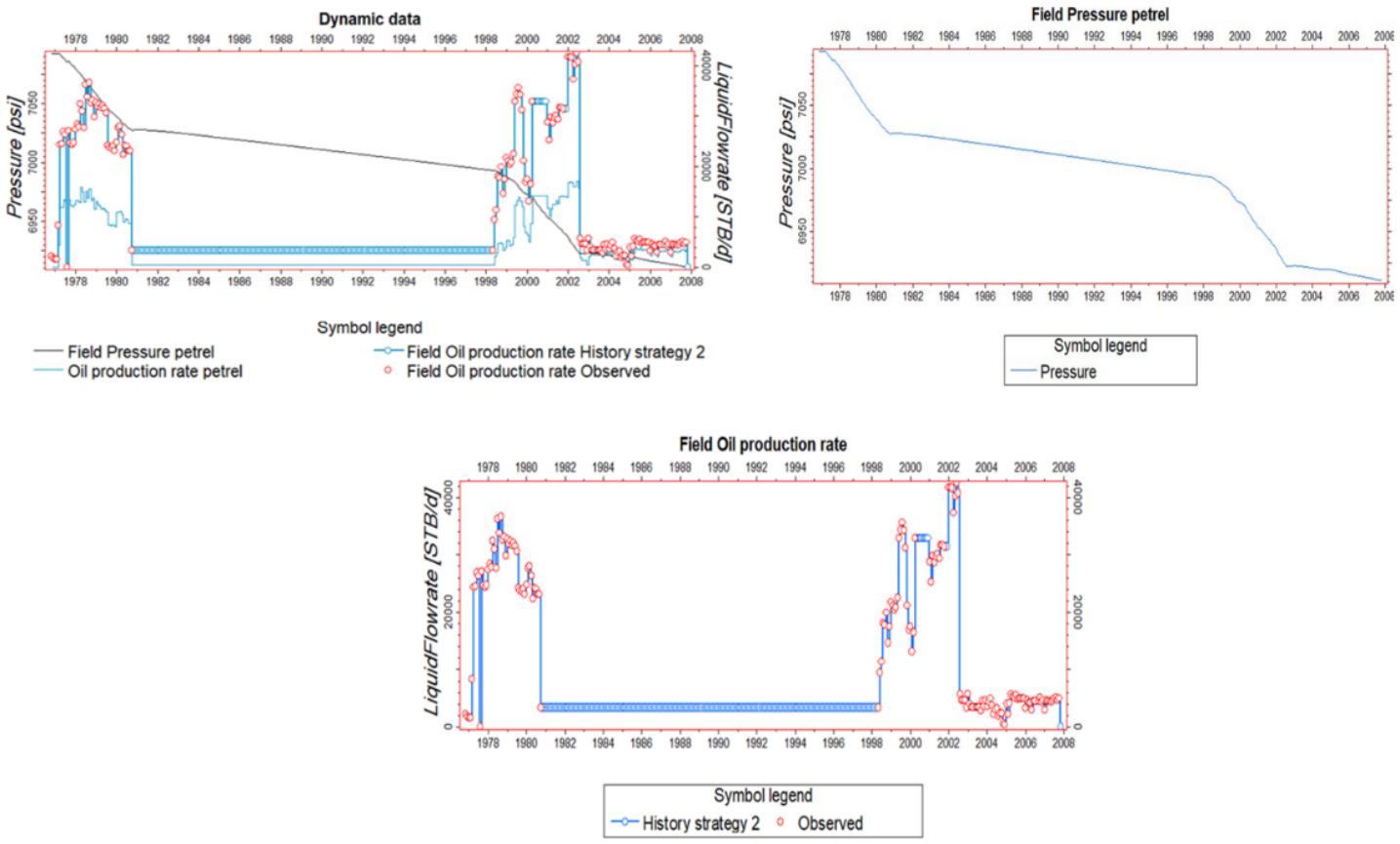

Figure 22—Field pressure calculated by petrel[TM].

Reservoir Performance. After history matching has been completed for the reservoir model, the subsequent step involves predicting the reservoir performance. The aim of performance prediction is to manage the field effectively and strive to maximize the recovery factor. Numerous wells in the Buzurgan oil field were drilled post-2003, a consequence of the Iraqi-Iranian war. These wells, along with others, were included in the history matching process. However, for the current study, there was insufficient data available for these wells. The performance of the Mishrif formation was predicted from 2007 to 2032 across various scenarios, which are summarized in **Table 10** for cumulative production and recovery.

Table 10—0il production rate and recovery for prediction performance.

Case	Cum-prod. MMSTB	Recovery
1	2750	0.5
2	2090	0.38
3	1650	0.3
4	2400	0.43

The base case, which serves as the foundation, was governed by the historical matching of the oil production rate, with additional control exerted by maintaining the bottom-hole pressure above the saturation pressure. The outcomes of this run, including the production rate and reservoir pressure, are depicted by the red figures (**Figures 23** and **24**), while the green curve represents the predictive performance of the reservoir when controlled by the water cut. It indicates a significant decline in production rate and a high water cut due to the decrease in bottom-hole pressure. Consequently, there is a need for high-capacity surface facilities and an injection process to mitigate the high pressure drop and enhance productivity and the recovery factor.

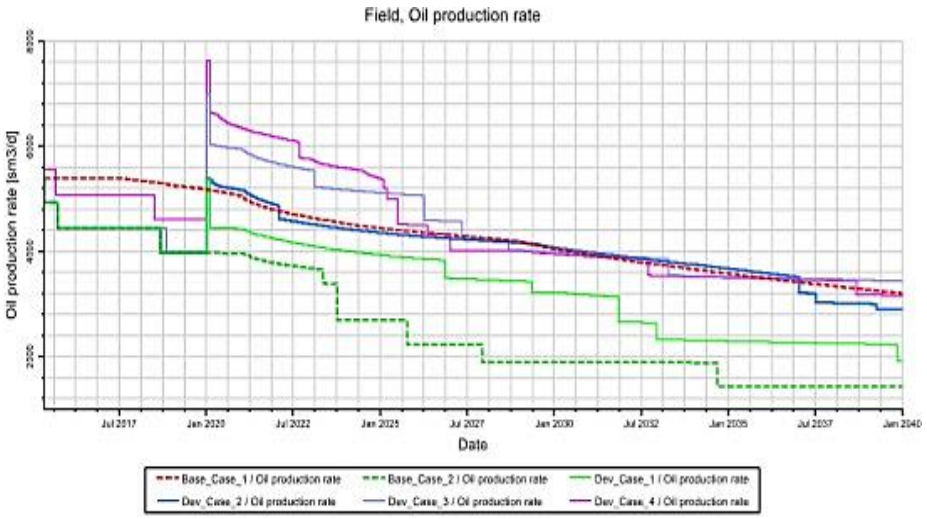

Figure 23—Prediction performance for the field oil production cases.

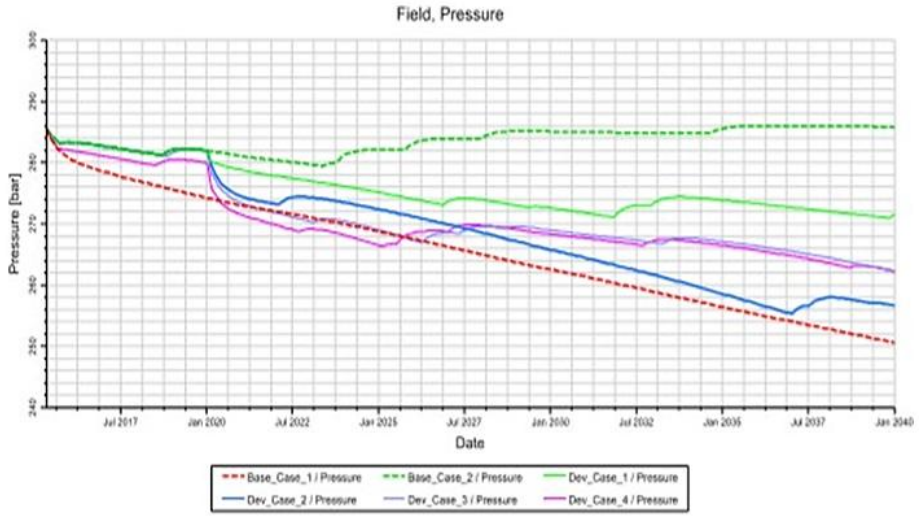

Figure 24—Prediction performance for the field oil production cases.

SOR Calculation. The reservoir simulation model was executed to estimate the cumulative oil production and oil recovery for various SOR (Solution Gas-Oil Ratio) values, based on the special core analysis reports for BU-3 and BU-4. These reports include oil-water relative permeability curves, each characterized by specific porosity and permeability values. By averaging these curves into a single curve, the relative permeability for oil and water was adjusted according to the changes in SOR. This process involved running simulations to study reservoir performance, with the aim of enhancing productivity and sustaining reservoir pressure above the saturation pressure. Figure 16 illustrates the average oil-water relative permeability curve derived from BU-3 and BU-4, where the oil relative permeability is zero. At this point, SW (Water Saturation) equals the cut-off value, and the SOR can be estimated using Eq. 7.

Figure 16 indicates that the cut-off for SW is 0.8, hence SOR equals 0.2. The relative permeability values were input into Petrel to conduct the simulation (**Table 11**). To obtain other SOR values, one can adjust the average curve in Figure 16 to a different SW cut-off (hypothetical) and perform a new simulation run.

Table 11—Oil production and recovery for each SOR.

SOR	Cumulative production (MMSTB)	SOR
0.15	1375	0.25
0.23	1045	0.19
0.28	825	0.15
Average (0.2)	1100	0.20

In the initial simulation run, with a water-oil ratio (SOR) of 0.15 and a water saturation (SW) cut-off of 0.85, achieving a good history match for the reservoir in question, the cumulative oil production amounted to 1,375 million stock tank barrels (MMSTB), and the recovery factor was 25% without any injection process. During the second simulation, with the SOR increased to 0.23 and the SW cut-off set at 0.77, the cumulative production decreased to 1,045 MMSTB, and the recovery factor was 19%. In the third simulation run, with an SOR of 0.28 and a SW cut-off of 0.72, the cumulative production further decreased to 825 MMSTB, and the recovery factor was 15% (Table 11). When these three scenarios were plotted on a single graph, the cumulative production was 1,100 MMSTB, and the recovery factor was 20%.

From the results, it is evident that recovery values decrease with an increase in SOR, and this decline correlates with changes in relative permeability at each SOR increment. Relative permeability to oil is higher in water-wet rock, which may lead to a higher ultimate oil recovery in mixed-wet and oil-wet rock. Consequently, as the SOR increases (indicating a decrease in water saturation), the rock becomes less water-wet, which lowers the relative permeability of oil and increases the relative permeability of water, thereby decreasing oil recovery.

Conclusions

Static and dynamic models for the Mishrif formation of the Buzurgan field have been constructed using commercial software, followed by history matching. Subsequently, predictions of future reservoir performance have been made. Some important conclusions can be drawn as follows.

1. The Mishrif reservoir, characterized by its carbonate composition and heterogeneity, is considered the best due to its excellent petrophysical properties. It is the primary reservoir, with the MB21 unit contributing 90% of the total production from the Mishrif Formation.
2. The carbonate rock exhibits scattering with a reasonable correlation on the permeability versus porosity plot. Consequently, this correlation was utilized in the simulation model for calculating permeability, as it provided good history matching when multiplied by a specific factor.
3. The initial oil in place is calculated using both static and dynamic models. There are differences between them regarding the values of porosity and saturation. In the static model, the calculation relies on porosity and water saturation data from well logs. In contrast, the dynamic model considers the effects of rock compaction, compressibility, and capillary pressure.
4. The oil-in-place in the static model is approximately 3.2 billion cubic meters, whereas in the dynamic model, it is about 2.1 billion cubic meters.
5. The value of recovery declines with an increased SOR, and this decline correlates with changes in relative permeability at each shift in SOR. Therefore, it is recommended to enhance the recovery factor through secondary mechanisms, utilizing injections to maximize productivity and maintain pressure above the saturation pressure.

Nomenclature

σ = Interfacial tension, dyne/cm
ρ_O = Oil density
ρ_w = Water density
V_p = Pore volume
$\emptyset$ = Porosity
BHP = Bottom hole pressure
Bo = Oil formation factor
BU = Buzurgan
C = Rock compressibility
CP = Centipoise
CPI = Computer-processed interpretation
Cum. = Cumulative
EOR = Enhanced oil recovery
FBHP = Flowing bottom hole pressure
GM = Gamma ray
GOR = Gas oil ratio
IP = Interactive Petrophysics software
J(sw) = J-function dimensionless
K = Permeability, md
KRO = Oil relative permeability
KRW = Water relative permeability
md = Millidarcy
N/G = Net to gross
OOIP = Original oil in place
OWC = Oil water contact
P_{ref} = Reference pressure
P = Cell pressure
P_c = Capillary pressure, psi
Phi = Porosity
P_o = Oil pressure
Prod. = Production
PVT = Pressure-Volume-Temperature
P_w = Water pressure
P_w (owc) = Reference water pressure at water oil contact
ROS = Remaining oil saturation
RS = Solution gas oil ratio, SCF/ STB
SCAL = Special core analysis
SCF = Standard cubic feet
SOR = Residual oil saturation
S_{orw} = Residual oil saturation or critical oil saturation
SP = Spontaneous potential
SSTVD = Sub sea true vertical depth
STB = Stock tank barrel
Std = Standard deviation
STOOIP = Stock tank original oil in place
S_W = Water saturation
S_{wc} = Connate or irreducible water saturation
TM = Trade mark
TVD = True vertical depth
V_B = Bulk volume (cell volume)

V_{pore} (p) = Pore volume at cell pressure
V_{pore} (Pref) = Pore volume at reference pressure
V_{sh} = Shale volume

Conflicting Interests

The author(s) declare that they have no conflicting interests.

References

Al Ibrahim, R. N., Al-Owaidi, M. R., Alnajen, F. M., et al. 2022. Investigation of the Geochemical Properties and Origin of the Crude Oils Accumulated in the Mishrif Reservoirs in the Zubair, Halfaya, and Buzurgan Oilfields, Southern Iraq. *The Iraqi Geological Journal* **2**(1):98-110

Al-Dujaili, A. N. 2023. Reservoir Rock Typing and Storage Capacity of Mishrif Carbonate Formation in West Qurna/1 Oil Field, Iraq. *Carbonates and Evaporites* **38**(4):83.

Al-Dujaili, A. N., Shabani, M., and AL-Jawad, M. S. 2021a. Characterization of Flow Units, Rock and Pore Types for Mishrif Reservoir in West Qurna Oilfield, Southern Iraq by Using Lithofacies Data. *Journal of Petroleum Exploration and Production Technology* **11**(1):4005-4018.

Al-Dujaili, A. N., Shabani, M., and AL-Jawad, M. S. 2021b. Identification of the Best Correlations of Permeability Anisotropy for Mishrif Reservoir in West Qurna/1 Oil Field, Southern Iraq. Egyptian Journal of Petroleum 30(3):27-33.

Al-Dujaili, A. N., Shabani, M., and AL-Jawad, M. S. 2023a. Effect of Heterogeneity on Recovery Factor for Carbonate Reservoirs: A Case Study for Mishrif Formation in West Qurna Oilfield, Southern Iraq. *Iraqi Journal of Chemical and Petroleum Engineering* **24**(3):103-111.

AL-Dujaili, A. N., Shabani, M., and AL-Jawad, M. S. 2023b. Effect of Heterogeneity on Capillary Pressure and Relative Permeability Curves in Carbonate Reservoirs: A Case Study for Mishrif Formation in West Qurna/1 Oilfield, Iraq. *Iraqi Journal of Chemical and Petroleum Engineering* **24**(1):13-26.

Al-Dujaili, A. N., Shabani, M., and Al-Jawad, M. S. 2023c. Lithofacies, Deposition, and Clinoforms Characterization Using Detailed Core Data, Nuclear Magnetic Resonance Logs, and Modular Formation Dynamics Tests for Mishrif Formation Intervals in West Qurna/1 Oil Field, Iraq. *SPE Reservoir Evaluation & Engineering* **26**(4):1258-1270.

Al-Dujaili, A.N., Shabani, M., and AL-Jawad, M.S. 2024. Lithofacies and Electrofacies Models for Mishrif Formation in West Qurna Oilfield, Southern Iraq by Deterministic and Stochastic Methods (Comparison and Analyzing). *Petroleum Science and Technology* **42**(13):1656-1684.

Alhusseini, A. K. and Hamd-Allah, S. 2022. Estimation of Initial Oil in Place for Buzurgan Oil Field by Using Volumetric Method and Reservoir Simulation Method. *The Iraqi Geological Journal* **2**(1):108-122.

Al-Janaee, H. M. and Al-shahwan, M. F. 2019. Estimation of Porosity and Permeability by Using Conventional Logs and NMR Log in Mishrif Formation/Buzurgan Oil Field. *Journal of Petroleum Research and Studies* **9**(3):75-89.

Aljawad, M. S., Hlaeel, M., Dawood, A. M. A., et al. 2017. Matching Well Test Data with Computer Model. *Journal of Petroleum Research & Studies* **23**(14):16-28.

Alkhateeb, A.M.A., 2019. A Comparative Study of Enhanced Oil Recovery for the Depleted Oil field in Iraq: A Simulation Modes Using Eclipse software (Master's thesis, Khazar University (Azerbaijan)).

Al-Mimar, H. S., Awadh, S. M., Al-Yaseri, A. A., et al. 2018. Sedimentary Units-Layering System and Depositional Model of the Carbonate Mishrif Reservoir in Rumaila Oilfield, Southern Iraq. *Modeling Earth Systems and Environment* **4**(1):1449-1465.

Al-Mimar, T. K., Al-Ameri, H. S., and Zumberge, J. 2015. Petroleum System Modeling and Risk Assessments of Ad'daimah Oil Field in Mesan Governorate. *Arabian Journal of Geosciences* **2015**(8):5739-5766.

Cao, X., Liu, Z., Hu, C., et al. 2024. Three-Dimensional Geological Modelling in Earth Science Research: An In-Depth Review and Perspective Analysis. *Minerals* **14**(7):686.

Chen, P., Bose, S., Selveindran, A., et al. 2023. Application of CCUS in India: Designing a CO_2 EOR and Storage Pilot in a Mature Field. *International Journal of Greenhouse Gas Control* **124**(1):103858.

Cobb, W. M. and Marek, F. J. 1998. Net Pay Determination for Primary and Waterflood Depletion Mechanisms. Paper presented at the SPE Annual Technical Conference and Exhibition, New Orleans, Louisiana, 27-29 September. SPE-48952-MS.

Deng, W. Q., Liang, T. B., Wang, W. Z., et al. 2023. A New Interacting Capillary Bundle Model on the Multiphase Flow in Micropores of Tight Rocks. *Petroleum Science* **25**(1): 1099-1122.

Ebraheem, M. O., Ibrahim, H. A., Ewida, H. F., et al. 2022. Identification of Hydrocarbon-Bearing Zones Within the Early Cretaceous Reservoir Rocks Using Well Logging and Seismic Reflection Data in Al-Baraka Field, West Komombo, Egypt. *Journal of Petroleum Science and Engineering* **218**(1):111037.

Eliebid, M., Mohamed, A., Arshadi, M., et al. 2024. Relative Permeability Hysteresis and Residual Trapping in Rough-Walled Fractures: An Experimental Investigation of the Effects of Flow Rate and Saturation History Using the Steady-State Approach. *Advances in Water Resources* **189**(1):104729.

Farouk, S., Sen, S., Ganguli, S. S., et al. 2021. Petrophysical Assessment and Permeability Modeling Utilizing Core Data and Machine Learning Approaches–A Study from the Badr El Din-1 Field, Egypt. *Marine and Petroleum Geology* **133**(1):105265.

Geffen, T. M., Owens, W. W., Parrish, D. R., et al. 1951. Experimental Investigation of Factors Affecting Laboratory Relative Permeability Measurements. *Journal of Petroleum Technology* **3**(4):99-110.

Hamdan, W. L. 2011. Petrel Software Modeling of the Mishrif Formation in Buzurgan Field. M.S. Thesis, University of Baghdad.

Hamdi, H., Ruelland, P., Bergey, P., et al. 2014. Using Geological Well Testing for Improving the Selection of Appropriate Reservoir Models. *Petroleum Geoscience* **20**(4):353-368.

Hurley, N. F., Zimmermann, R. A., and Pantoja, D. 1998. Quantification of Vuggy Porosity in a Dolomite Reservoir from Borehole Images and Core, Dagger Draw Field, New Mexico. Paper presented at the SPE Annual Technical Conference and Exhibition, New Orleans, Louisiana, 27-29 September. SPE-49323-MS.

Ji, L., Xu, F., Lin, M., et al. 2023. Rapid Evaluation of Capillary Pressure and Relative Permeability for Oil–Water Flow in Tight Sandstone Based on a Physics-Informed Neural Network. *Journal of Petroleum Exploration and Production Technology* **13**(12):2499-2517.

Leverett, M. C. and Lewis, W. B. 1941. Steady Flow of Gas-Oil-Water Mixtures Through Unconsolidated Sands. *Transactions of the AIME* **142**(1):107-116.

Liu, W., Li, Y., Liu, Q., et al. 2023. Roles of Gypsum/Salt-Bearing Sequence in Hydrocarbon Accumulation and Storage. *Energy Geoscience* **4**(1):93-102.

Mahmud, H. B., Hisham, M. H. B. M., Mahmud, W. M., et al. 2020. Petrophysical Interpretations of Subsurface Stratigraphic Correlations, Baram Delta, Sarawak, Malaysia. *Energy Geoscience* **1**(3):100-114.

Mohammed, M. M., Salih, H. M., and Mnaty, K. H. 2022. 3D Reservoir Modeling of Buzurgan Oil Field, Southern Iraq. *Iraqi Journal of Science* **3**(1):596-607.

Muskat, M. 1949. Calculation of Initial Fluid Distributions in Oil Reservoirs. *Transactions of the AIME* **179**(1):119-127.

Natvig, J., Dias, D., Bratvedt, F., et al. 2023. Multiscale Reservoir Simulation of High-Resolution Models. Paper presented at the SPE Reservoir Simulation Conference, Galveston, Texas, USA, 21-23 March. SPE-212231-MS.

Oil Exploration Company- Geophysical. 1980. Seismic Study for Buzergun and Fauqa Oil Field. Ministry of Oil, Final Well Reports.

Qassamipour, M., Khodapanah, E., and Tabatabaei-Nezhad, S. A. 2020. Determination of Cutoffs by Petrophysical Log Data: A New Methodology Applicable to Oil and Gas Reservoirs. *Energy Sources, Part A: Recovery, Utilization, and Environmental Effects* **3**(1):1-14.

Satter, A. and Iqbal, G. M. 2015. Reservoir Engineering: The Fundamentals, Simulation, and Management of Conventional and Unconventional Recoveries. New York, USA: Gulf Professional Publishing.

Siripatrachai, N., Ertekin, T., and Johns, R. T. 2017. Compositional Simulation of Hydraulically Fractured Tight Formation Considering the Effect of Capillary Pressure on Phase Behavior. *SPE Journal* **22**(4):1046-1063. SPE-179660-PA.

Sugiharto, Y. E., Ralphie, B., and Johare, D. 2020. Using Agile Saturation Distribution to Turn the Models into Democratic Knowledge for Faster Clastic Subsurface Characterization. Paper presented at the Abu Dhabi International Petroleum Exhibition and Conference, Abu Dhabi, UAE, 9-11 November. SPE-203477-MS.

Tariq, Z., Mahmoud, M., and Abdulraheem, A. 2021. Machine Learning-Based Improved Pressure–Volume–Temperature Correlations for Black Oil Reservoirs. *Journal of Energy Resources Technology* **143**(11):113003.

Teklu, T. W., Brown, J. S., Kazemi, H., et al. 2013. Residual Oil Saturation Determination–Case Studies in Sandstone and Carbonate Reservoirs. Paper presented at the SPE Europec featured at EAGE Conference and Exhibition, London, UK, 10-12 June. SPE-164825-MS.

Tohidi, E., Hesan, M., Azad, A., et al. 2024. Implementing Pore Size Distribution into Saturation Height Function Modelling of Reservoir Rock Types: A Case Study on a Carbonate Gas Reservoir. *Gas Science and Engineering* **121**(1):205188.

Tsuji, T., Jiang, F., and Christensen, K. T. 2016. Characterization of Immiscible Fluid Displacement Processes with Various Capillary Numbers and Viscosity Ratios in 3D Natural Sandstone. *Advances in Water Resources* **95**(1):3-15.

Ugwu, I. J., Okobiebi, O. O., Overare, B., et al. 2023. 3D Static Reservoir Modelling: a Case Study of the Izu Field, Coastal Swamp Depobelt, Niger Delta Basin. *Arabian Journal of Geosciences* **16**(1): 42:54.

Vishnumolakala, N., Zhang, J., and Ismail, N. B. 2020. A Comprehensive Review of Enhanced Oil Recovery Projects in Canada and Recommendations for Planning Successful Future EOR Projects. Paper presented at the SPE Canada Heavy Oil Conference, Virtual, 24-25 September. SPE-199951-MS.

Worthington, P. F. and Cosentino, L. 2005. The Role of Cutoffs in Integrated Reservoir Studies. *SPE Reservoir Evaluation & Engineering* **8**(4):276-290. SPE-84387-PA.

Zeyghami, M. and Taghizadeh Sarvestani, M. 2023. A Comprehensive Methodology for Reservoir Cut-Off Determination. *Journal of Petroleum Exploration and Production Technology* **13**(7):1551-1573.

Abdulkareem Abbas Khalil is an Assistant Professor at the University of Kerbala. He holds a PhD in Petroleum Engineering from Baghdad University (2007), with MSc (1990) and BSc (1987) degrees in the same field from the same university. His research interests focus on petroleum engineering, including oil well drilling operations, horizontal and directional drilling, oil well control, and well logging.

Hussain Ali Baker serves as an Assistant Professor at Almaaqal University in Basrah, Iraq. He obtained his PhD in Petroleum Engineering from Baghdad University (2000), complemented by an MSc (1989) and a BSc (1981) in Petroleum Engineering from the same institution. His key research areas include phase behaviour, well testing, applied reservoir engineering, and enhanced oil recovery (EOR).

Hiba Alaa Naseef is affiliated with the Petroleum Engineering Department at the University of Baghdad. She earned her MSc in Petroleum Engineering from Baghdad University (2020) and a BSc in the same field from the university (2016). Her research focuses on reservoir engineering and enhanced oil recovery.

Ahmed N. AL- Dujaili is an Assistant Professor at Amirkabir University of Technology in Tehran, Iran, and a Visiting Professor at Kerbala University. He holds a PhD in Petroleum Engineering from Amirkabir University of Technology (2022), with an MSc (2015) and a BSc (1992) in Petroleum Engineering from Baghdad University. His broad research interests include petroleum exploration, reservoir engineering, drilling engineering, petroleum geology, EOR, and water resources.